

Physics of X-ray Microbeam Radiation Therapy

Stefan Bartzsch^{1, 2}, Stéphanie Corde^{3, 7}, Jeffrey Crosbie⁴, Liam Day⁴, Mattia Donzelli^{5, 6}, Michael Krisch⁵, Michael Lerch^{7, 8}, Paolo Pellicoli^{5, 9, 10}, Lloyd Smyth¹¹, and Moeava Tehei^{7, 8}

¹Technical University of Munich, School of Medicine, Klinikum rechts der Isar, Department of Radiation Oncology, Munich, Germany

²Helmholtz Centre Munich, Institute for Radiation Medicine, Munich, Germany

³Prince of Wales Hospital, Radiation Oncology Department, Randwick NSW Australia

⁴School of Science, RMIT university, Melbourne, Australia

⁵The European Synchrotron Radiation Facility, Grenoble, France

⁶The Institute of Cancer Research, London, UK

⁷Centre for Medical Radiation Physics, University of Wollongong, Wollongong NSW Australia

⁸Illawarra Health and Medical Research Institute, University of Wollongong, Australia

⁹EA RSRM 7442, Grenoble Alpes University, Grenoble, France

¹⁰Swansea University, Swansea, UK

¹¹Department of Obstetrics & Gynaecology, University of Melbourne, Australia

May 28, 2019

Abstract

25 In the last 25 years Microbeam Radiation Therapy (MRT) has emerged as a
26 promising alternative to conventional radiation therapy at large, third gener-
27 ation synchrotrons. In MRT, a multi-slit collimator modulates a kilovoltage
28 X-ray beam on a micrometer scale, creating peak dose areas with unconvention-
29 ally high doses of several hundred Grays separated by low dose valley regions,
30 where the dose remains well below the tissue tolerance level. Pre-clinical evi-
31 dence demonstrates that such beam geometries lead to substantially reduced
32 damage to normal tissue at equal tumour control rates and hence drastically
33 increase the therapeutic window. Although the mechanisms behind MRT are
34 still to be elucidated, previous studies indicate that immune response, tumour
35 microenvironment, and the microvasculature may play a crucial role. Beyond
36 tumour therapy, MRT has also been suggested as a microsurgical tool in neuro-
37 logical disorders and as a primer for drug delivery.

38 The physical properties of MRT demand innovative medical physics and en-
39 gineering solutions for safe treatment delivery. This article reviews technical
40 developments in MRT and discusses existing solutions for dosimetric validation,
41 reliable treatment planning and safety. Instrumentation at synchrotron facili-
42 ties, including beam production, collimators and patient positioning systems, is
43 also discussed. Specific solutions reviewed in this article include: dosimetry tech-
44 niques that can cope with high spatial resolution, low photon energies and ex-
45 tremely high dose rates of up to 15 000 Gy/s, dose calculation algorithms - apart
46 from pure Monte Carlo Simulations - to overcome the challenge of small voxel
47 sizes and a wide dynamic dose-range, and the use of dose-enhancing nanopar-
48 ticles to combat the limited penetrability of a kilovoltage energy spectrum. Fi-
49 nally, concepts for alternative compact microbeam sources are presented, such
50 as inverse Compton scattering set-ups and carbon nanotube x-ray tubes, that
51 may facilitate the transfer of MRT into a hospital-based clinical environment.

52 Intensive research in recent years has resulted in practical solutions to most
53 of the technical challenges in MRT. Treatment planning, dosimetry and patient
54 safety systems at synchrotrons have matured to a point that first veterinary
55 and clinical studies in MRT are within reach. Should these studies confirm the
56 promising results of pre-clinical studies, the authors are confident that MRT
57 will become an effective new radiotherapy option for certain patients.

1 Introduction

Despite the technical and biological advances of modern radiotherapy, there are many types of cancer that have not seen significant improvements in prognosis. For example, paediatric diffuse intrinsic pontine glioma, an aggressive brainstem tumour, has a survival rate of less than 10% at two years following diagnosis^[1]. Locally advanced pancreatic cancer and glioblastoma multiforme both have survival rates of less than 10% at five years^[2,3]. Chondrosarcoma, a notoriously aggressive cancer of cartilaginous cells, is usually resistant to both chemotherapy and conventional radiotherapy, making surgical resection – often amputation – the main effective treatment option^[4–6]. In these scenarios, the intrinsic characteristics of the disease, or the sensitivity of surrounding organs to radiation, hinders any opportunity for lasting disease control.

These dismal outcomes suggest that a paradigm shift could be required to improve prognosis and perhaps provide the possibility of cure. Spatially fractionated radiotherapy using microbeams is a radical departure from the physical properties and radiobiological principles of conventional radiotherapy. The purpose of this review is to explore the physics and technical developments fundamental to the field of microbeam radiotherapy (MRT).

1.1 Paradigms in modern radiation oncology

The broad aim of conventional radiotherapy is to safely deliver the highest possible homogenous dose to the target volume. This objective is primarily achieved through the temporal fractionation of dose and geometric dose-conformity to the target. Linear accelerators are the workhorse of modern radiotherapy clinics globally, facilitating the treatment of a diverse range of tumours in virtually any location in the body. Most linear accelerators generate mega-electron-volt (MeV) x-rays and electrons, operate at a dose rate in the order of 0.1 Gy/s and produce homogenous fields of radiation that can be collimated or modulated to optimise the geometry of dose-distributions in tissue.

Early in the 20th century, the first radiotherapy treatments were delivered as a large single fraction and associated with significant morbidity and physical disfigurement. These toxic effects were the backdrop for one of the most fundamental developments in radiation oncology; temporal fractionation. In the early 1920s, Claudius Regaud and his French compatriot Henri Coutard demonstrated that healthy tissue could better tolerate a course of radiotherapy when delivered as a series of several smaller doses over consecutive days, without compromising tumour control^[7]. Splitting a large radiation dose into multiple smaller fractions capitalises on four of the ‘Five Rs of Radiotherapy’^[8]. In healthy tissue, there is opportunity for the repair of non-lethal DNA damage and repopulation of the normal cell niche. Simultaneously, the processes of reoxygenation and cell-cycle redistribution increase tumour radio-sensitivity. Temporal fractionation gained acceptance in the wider radiation therapy community by the 1930s and remains a cornerstone of modern radiation oncology.

The therapeutic effect of radiotherapy is also fundamentally maximised by increasing the geometric conformity of dose to the tumour target. Given that healthy tissue surrounding the tumour limits the maximum dose deliverable, the high-dose region is sculpted as closely as possible to the target volume. The target typically includes the gross tumour volume plus an additional margin

1
2
3
4
5
6
7
8
9
10
11
12
13
14
105 in normal tissue to account for sub-clinical spread and uncertainties in target
16 position. The majority of technical advancements in modern radiation oncology
17 – intensity modulation^[9,10], image-guidance^[11,12], motion-management^[13,14],
18 particle therapy^[15] – have revolved around improving the conformity of dose to
19 the target, reducing collateral damage to healthy tissue and facilitating dose-
20 escalation.
110

15 1.2 Spatially fractionated radiotherapy

16
17 The concept of spatial fractionation is built on the dose-volume effect; that the
18 tolerance of normal tissue to radiation increases as the irradiated volume of
19 that specific tissue is reduced^[16–18]. Albert Köhler first conceived the idea of
20 applying spatial fractionation to radiotherapy in 1909. Köhler showed that skin
21 toxicity could be reduced using ‘grid therapy’, where a 3 mm² grid of woven
22 iron wire was pressed closely to the skin of patients during kilovoltage irradiation^[19].
23 Today, macroscopic grid therapy using megavoltage x-rays from a linear
24 accelerator is used to de-bulk large and advanced tumours prior to conventional
25 radiation therapy (RT)^[20], however this technique is not widely used.

26 Several forms of spatially fractionated radiotherapy, including MRT, are
27 currently in pre-clinical development. While MRT is the focus of this review,
28 there are other noteworthy modalities including minibeam radiotherapy, which
29 utilises arrays of sub-millimetre (0.4 – 0.7 mm) planar beams of x-rays^[21–23]
30 or protons^[24,25], and microchannel irradiation using arrays of x-ray or proton
31 microbeams^[26,27].
32

33 1.3 Microbeam radiotherapy

34
35 At present, MRT is the most extensively investigated modality that employs
36 spatial dose-fractionation. Microbeams were first used in medicine in the 1960s
37 to understand the effects of cosmic radiation. At that time, Zeman et al.^[28]
38 reported that the tolerance of mouse brain tissue to a single beam of deuterons
39 could be increased from 140 Gy to 4000 Gy when reducing the diameter of the
40 beam from 1 mm to 25 μm . While the work of Zeman and colleagues exemplified
41 the dose-volume effect, it was not until the late 1980s that true spatial dose-
42 fractionation using microbeams was demonstrated.

43 MRT was first explored by Daniel Slatkin and colleagues at the Brookhaven
44 National Laboratory in the late 1980s and early 1990s^[29,30]. MRT has been in
45 pre-clinical development at a small number of synchrotrons across the world ever
46 since, including the European Synchrotron Radiation Facility (ESRF) (Grenoble,
47 France), SPring-8 (Hyogo Prefecture, Japan), the Australian Synchrotron
48 (Melbourne, Australia) and the Canadian Light Source (Saskatoon, Canada).
140

49 In MRT, spatial dose-fractionation is achieved on a microscopic scale. Fields
50 are characterised by an array of 25 to 100 μm wide, quasi-parallel, micro-planar
51 beams that have a centre-to-centre spacing of 100 to 400 μm ^[31]. This kind of
52 array creates an inhomogeneous, periodically alternating dose profile of ‘peaks’
53 and ‘valleys’ (Figure 1). In-beam doses (peaks) can be up to 100 times higher
54 than the dose between the beams (valleys) due to scatter^[32]. In pre-clinical
55 *in vivo* studies, peak to valley dose ratios (PVDRs) are more commonly in the
56 range of 20 to 50^[33–37]. The physical characteristics of MRT are discussed more
57 thoroughly in sections 2 and 4.
150

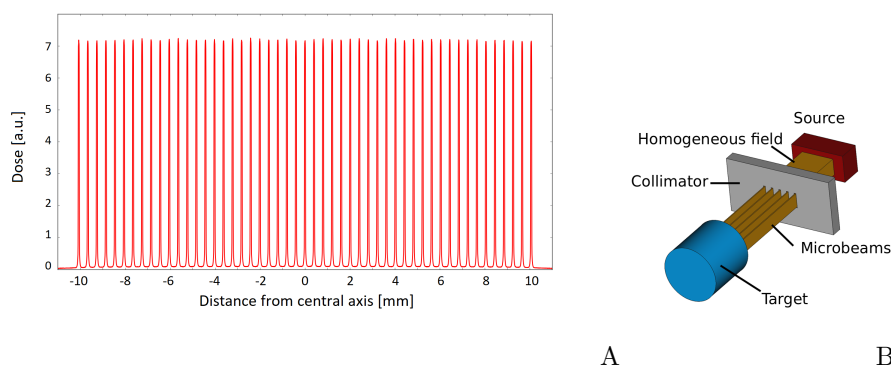


Figure 1: A: A typical beam profile of microbeams, simulated for a $20\text{ mm} \times 4\text{ mm}$ field in 10 mm depth in water at the imaging and medical beam-line of the Australian Synchrotron. The principle of microbeam generation is shown in B. A collimator shapes microbeams from a homogeneous x-ray beam.

Peak doses used in pre-clinical MRT experiments usually fall in the range of 100 to 1000 Gy^[33,38–40]. These extremely high peak doses are tolerated by a range of healthy tissues with minimal structural or physiological deficits^[33,35,40–42]. In addition to the remarkable tolerance of normal tissue to peak doses, pre-clinical studies show that MRT can slow tumour growth and even facilitate tumour control despite not irradiating the entire tumour with a uniform field^[43–45].

While compact MRT delivery systems have also been developed^[46,47] and are reviewed in section 6, the properties of synchrotron radiation are optimal for delivering the peak-valley dose-distribution intrinsic to MRT^[29]. Firstly, the keV x-ray energy minimises the range of secondary electrons in the valley region, preserving a high PVDR. Secondly, the ultra high dose rate mitigates the effects of physiological tissue motion, including the cardio-synchronous pulsation of blood vessels and respiration. Lastly, minimal beam divergence is required to maintain the array geometry on a microscopic scale. The high dose-rates and peak doses, in combination with microscopic spatial resolution, makes physical methods of dosimetry very demanding. Techniques to facilitate synchrotron-based MRT dosimetry are discussed in Section 3.

There are a number of mechanisms that have been proposed for the therapeutic efficacy of MRT. Firstly, normal tissue retains its cellular architecture and the ability to launch a coordinated repair response following MRT while certain tumour tissues (e.g. breast tumour) demonstrate marked cellular migration and reduced proliferative capacity^[48]. Secondly, MRT exerts differential transcriptional effects on tumour and normal tissue, with differences in key pathways relating to immunity and inflammation^[49,50]. The regulation of inflammation and immune response is also different when comparing tissue irradiated using MRT versus conventional RT^[51–53], which further highlights the potential importance of these pathways to the therapeutic effect of MRT. Thirdly, tumour micro-vasculature has a greater radio-sensitivity to MRT compared to normal brain micro-vasculature^[54,55], which has implications for vascular permeability and the delivery of micro-nutrients, cellular mediators of damage repair and immune cell recruitment. Finally, the ultra-high dose-rate of MRT – several

1
2
3
4
5
6
7
8 hundred^[56] to several thousand^[57] Gray per second – may contribute to im-
9 proved normal tissue sparing via what is now known as the FLASH effect^[58].

10 The degree to which the FLASH effect might contribute to the normal tissue
11 sparing characteristics of MRT has not yet been elucidated. However, as a
12 stand-alone technique, broad-beam FLASH radiotherapy at dose-rates greater
13 than 40 Gy/s reduces lung fibrosis^[58] and mitigates brain injury^[59,60] in rodent
14 models compared to irradiation at conventional dose-rates (0.1 Gy/s). These
15 tissue-sparing phenomena have since been reproduced in large animal models,
16 with pet cats bearing spontaneous facial cancers also experiencing favourable
17 tumour control outcomes following treatment with FLASH radiotherapy^[61].

18 19 20 **1.4 Potential clinical applications of MRT in medicine**

21 MRT is currently in a pre-clinical phase and to date, no human patients have
22 been treated with MRT. The current challenge is to develop safe protocols
23 that maximally exploit the unique radiobiological properties of MRT. A di-
24 verse range of potential clinical applications of MRT have been identified and
25 explored through *in vivo* studies.

26 The biological rationale for MRT as a stand-alone, combination, or neoadju-
27 vant treatment has been established in pre-clinical studies. Significant technical
28 developments in the realm of medical physics are required to facilitate future
29 pre-clinical and veterinary studies, and ultimately, the first human trials of
30 MRT. These developments are the focus of this review.

31 32 33 **1.4.1 MRT as a boost for conventional radiotherapy**

34 Schültke et al.^[62] propose that MRT could be used as an integrated boost
35 within a conventional radiotherapy regimen. Here, the valley dose would match
36 the daily prescribed conventional radiotherapy dose while the peaks would act as
37 a simultaneous boost to enhance tumour control^[62]. Bouchet et al.^[45] provide a
38 rationale for this approach by demonstrating better overall survival, in a rodent
39 glioma model, following MRT compared to broad-beam irradiation when the
40 MRT valley dose was matched to the broad-beam dose.
41
42
43
44

45 **1.4.2 MRT as a primer for drug delivery**

46 The previous potential applications of MRT largely draw on the normal tissue
47 sparing properties of spatial fractionation, allowing for dose-escalation to the
48 tumour. However, the differential effect of MRT on tumour and normal mi-
49 crovasculature^[55] makes MRT a potentially potent primer for drug delivery by
50 inducing a window of enhanced vascular permeability in the tumour^[63]. Simi-
51 larly, the immunomodulatory properties of MRT^[50,52,64] could be exploited in
52 combination with immunotherapy. Pre-clinical studies have demonstrated the
53 synergistic effect of MRT in combination with a range of drugs^[65,66] and im-
54 munotherapy^[67]. However, the optimal dose and timing of MRT in this setting,
55 and the choice of ideal chemo- or immunotherapeutics to test in combination,
56 remains to be determined.
57
58
59
60

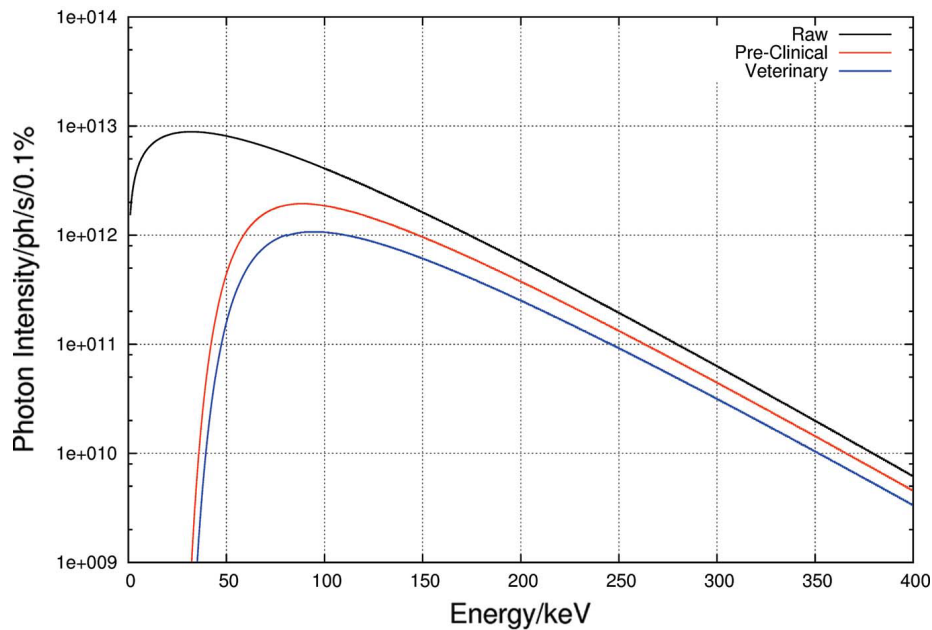


Figure 2: Typical unfiltered and filtered wiggler spectrum for MRT applications. Example of ID17 at the ESRF. Figure was taken from^[77].

1.4.3 MRT as a micro-surgical tool in neurological disorders

Alongside possible applications in radiation oncology, MRT has the potential to alleviate the symptoms of neurological conditions. In this context, MRT could be used to deliberately transect key neuronal pathways or ablate highly localised regions of the brain in order to modulate or suppress the networks responsible for abnormal movement^[68,69]. Proof of principle data supporting these neurosurgical applications of MRT exists in pre-clinical models of spinal cord injury^[70] and epilepsy related to the somatosensory cortex^[71]. Epilepsy induced by mesial temporal sclerosis may also benefit from this application of MRT^[72].

2 Technical development and engineering

2.1 Properties of synchrotron radiation

The discovery of synchrotron radiation in 1946^[73] and the subsequent development of synchrotron radiation research centers around the world have revolutionized x-ray science. Modern synchrotron sources at dedicated storage rings have a brilliance (number of photons/s/mm²/mrad² within a bandwidth of 0.1%) in the order of 10²¹ as compared to 10⁷ for conventional x-ray tubes^[74–76]. Currently, the most appropriate x-ray source for MRT is a so-called wiggler (as opposed to a bending magnet or an undulator), which provides a continuous high photon flux spectrum and a sufficiently large horizontal radiation fan for the desired size of the radiation field (see Figure 2). The main considerations for the optimization of the MRT photon spectrum relate to (i) maximising the pho-

1
2
3
4
5
6
7
8 245 ton flux to allow for the required dose rate delivery; (ii) providing the necessary
9 x-ray energy to reach deep-lying targets, and (iii) maximising the peak-to-valley-
10 dose ratio (PVDR). In this context, photon energies below 50 keV are considered
11 not useful; these are therefore filtered out by the insertion of a set of absorption
12 filters (see below).

13 250 On the other hand, extensive MC calculations of an array of micro-beams
14 revealed that a mean photon energy around 100 - 150 keV gives the best com-
15 promise between a well-defined peak dose profile with a sharp fall-off towards
16 the valley dose region^[78,79] (see section 4).

17 18 **2.2 General beamline lay-out**

19
20 255 The typical beamline lay-out for MRT has been described in detail in the
21 past^[80-83]. Standard components comprise horizontal and vertical slits to re-
22 duce the heatload and to define the broad and MRT beam dimensions. A filter
23 train eliminates the low-energy part of the spectrum. To monitor the beam
24 stability, ionization chambers (IC) or a Compton chamber beam monitor are in-
25 260 stalled. Preclinical studies with small and large animals require slightly different
26 conditions in terms of spectral filtering, intensity, and dose monitoring^[77,80,81].

27 28 **2.3 Fast shutters**

29
30 The radiation dose delivered to the target, needs to be accurately controlled
31 in order to prevent unnecessary damage to surrounding, normal tissues. Im-
32 265 plementation of a dedicated photon shutter system, combined with a reliable,
33 redundant interlock system, prevents any excessive dose delivery.

34 The system, implemented on the biomedical beamline ID17 at the ESRF,
35 consists of a standard photon absorber, followed down-stream by a fast shutter
36 device^[84]. The measured error in the exposure time of the fast shutter amounts
37 270 to ± 0.5 ms, which results in a 1 % error for typical exposure times of 50 ms.

38 39 **2.4 Multislit collimator**

40
41 One of the key elements in MRT is the Multislit Collimator (MSC) since the
42 mechanical regularity of such devices is the most important property required
43 to produce an array of identical microbeams. Following first designs^[85,86], the
44 275 currently most utilized MSC is a single slit device composed of 8 mm thick
45 blocks of tungsten carbide (WC), presenting 125, three mm high, and 50 μm wide
46 equidistant slits to the incoming seamless x-ray beam, regularly repeated with
47 a uniform pitch of 400 μm ^[87]. The MSC chamber is mounted on a rotational
48 stage, equipped with a motorized translation in the vertical direction and in
49 280 the horizontal direction perpendicular to the x-ray beam, for rapid alignment.
50 Schematic drawings of the MSC and its assembly are shown in Figure 3.

51 An extensive characterization of the MSC led to 404 μm (SD 10 μm) for the
52 regularity of the slit spacing, and 51.8 μm (SD 1.1 μm) for the slit width.

53 54 **2.5 Sample goniometer and patient positioning system**

55
56 285 Sample and patient positioning systems for MRT are different from positioning
57 systems used in conventional RT due to the use of a fixed horizontal beam rather

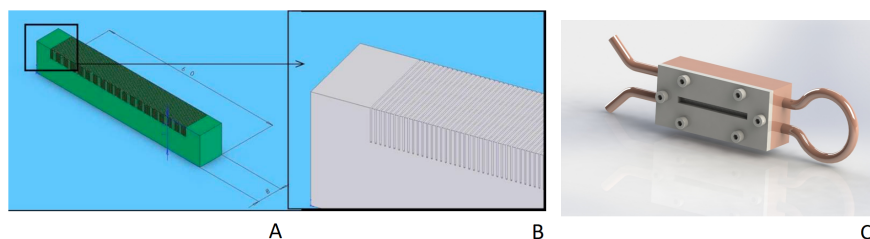


Figure 3: A: schematic drawing of a MSC with $100\ \mu\text{m}$ slit width and a pitch of $400\ \mu\text{m}$ and B: zoom of the assembly; C: MSC embedded inside the copper block with its pipes for water cooling.

than a rotating gantry. In addition, the limited beam height requires the vertical translation of a target through the beam during irradiation. At the ESRF a kappa-type goniometer manufactured by Huber (Germany) is installed^[86,88] on top of a vertical translational stage (see figure 4A). Its loading capacity is 35 kg, and the z-stage allows for a total vertical movement of 150 mm at a maximum linear speed of 150 mm/s. The accuracy in velocity of the translational stage allows for a dose delivery with an accuracy of 5%. In view of the upcoming human clinical trials, a conceptual design study was performed for a patient positioning system (see figure 4B). At the BMIT beamline of the Canadian Light Source (CLS) in Saskatoon, Canada, a large animal positioning system (LAPS) is installed capable of holding samples up to 907 kg^[83]. The LAPS can move at vertical velocities of up to 200 mm/s at 1% accuracy and a spatial accuracy of $100\ \mu\text{m}$. On top of the LAPS a kappa-type goniometer with a loading capacity of up to 120 kg can be installed for 3-axis sample positioning^[89] (see figure 4C).

More recently, the IMBL at the Australian Synchrotron have installed two robotic positioning devices; a so-called Large Animal Positioning System (LAPS) and a Patient Positioning System (PPS) (see figure 4D). These robots are located in the long beamline known as Hutch 3B where phase contrast radiography, tomography, and some radiotherapy experiments take place. There are also plans to install another robotic patient positioning device on the near beamline (Hutch 2B) in the future. These robots are similar in scale to the positioning systems used in fixed-beam proton therapy facilities. Whilst these robotic devices are primarily used to image large animals and humans, they can also be used to translate patients vertically through a therapeutic beam. Commissioning work is taking place in 2019 to verify and validate the use of the LAPS and PPS for veterinary trials of synchrotron radiotherapy.

An irradiation sequence starts with the prepositioning of the target, and taking into consideration location marks obtained during prior imaging sessions. By means of the z-stage, the target is driven to the start position, and when the irradiation scan is triggered, the target accelerates vertically to reach the steady speed as chosen by the operator. The fast shutter opens and closes precisely at pre-determined positions depending on the volume to be treated. The target then decelerates and stops, and returns to its start position. The target may be re-oriented in another direction and a further irradiation sequence may start.

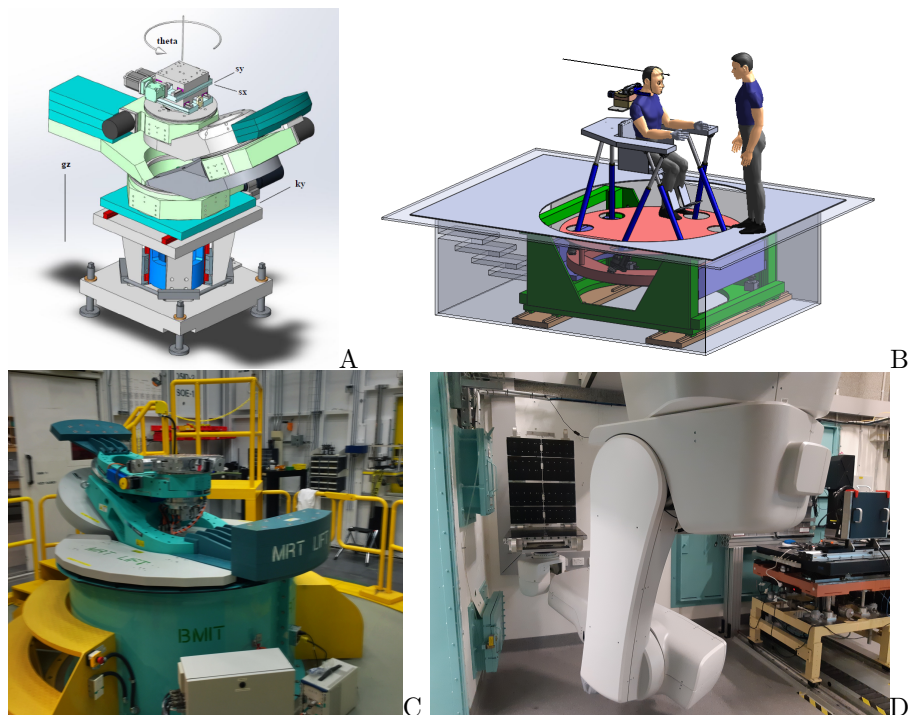


Figure 4: Current MRT kappa type goniometer in the MRT experimental hutch for preclinical research in MRT (A) and design of the future patient positioning and irradiation system for MRT clinical trials (B) at the ESRF. A stage for horse MRT trials at the Canadian Lightsource (C). A robotic patient positioning system (PPS) and a large animal positioning system (LAPS) has been installed at the Australian Synchrotron (D).

2.6 Image-guidance

Image-guidance is a well established technique in conventional RT to increase the spatial precision of a RT treatment. Various imaging techniques (fan and cone beam CT, x-ray projection imaging, MRI) can be used to verify the patient anatomy for planning and the patient set-up prior to and during the treatment. The special circumstances at the currently available radiation sources for MRT have lead to the development of specialised techniques and protocols for image-guidance adapted to the fixed horizontal beam geometry at synchrotron facilities.

The first image-guided MRT experiment was reported in 2010 by Serduc et al.^[90] at the ESRF beamline ID17. Their image-guidance protocol used the same radiation source for rat imaging and irradiation. To reduce the x-ray beam intensity and energy, the wiggler gap was opened and additional absorbers were placed in the beam for imaging. The rat imaging was carried out step by step acquiring 1 mm high frames while the animal was translated gradually upwards. A graphical user interface (GUI) displayed the full x-ray image and assisted in the positioning of the animal in the beam using bone structures of the skull as reference points for atlas-based alignment. The rotation was not corrected in this protocol which was used for radiosurgery of somatosensory cortex and thalamus of GAERS rats to investigate the effect of microbeams on epileptic seizures. The same protocol was successfully applied by others, e.g. Romanelli et al.^[91].

Zhang et al.^[92] used a combination of x-ray projection imaging and pre-irradiation MRI for tumour-bearing rats. They located the tumour on an MRI-image and performed an image-registration of sagittal MRI planes with projection images taken of the animal mounted on the irradiation stage of a carbon nano tube (CNT) based irradiator^[93]. The applied re-positioning consisted of a translation of the animal in the image plane without any correction for the rotation.

The protocol developed by Nemoz et al.^[94] at the ESRF was the first to acquire a full tomographic scan of the region of interest of a rat while the animal is immobilized on the treatment stage. Using a pink synchrotron radiation beam as described in Serduc et al.^[90], a CT of the animal head was acquired in 5 slices of 2 mm height each with a pixel size of 100 μm . Iodine as contrast agent was used to enhance tumour contrast on the CT images and the imaging spectrum was adjusted to match the iodine K-edge at 33 keV.

At the Australian Synchrotron Pelliccia et al.^[95] developed a small animal image-guidance protocol which employs monochromatic synchrotron radiation for sample imaging. The use of a double-crystal Laue monochromator introduced a 20 mm shift between treatment and imaging beam which required vertical translation of the target in between the two procedures.

The sample imaging was done during a continuous vertical translation through the laminar x-ray beam, while a silicon detector acquired a series of images which were then tiled together to a full-field representation of the sample. To gather additional information on the sample, a CT slice of the plane selected on the projection image can be taken, similar to the procedure of Nemoz et al.^[94]. The image quality can be improved by relying on phase contrast images^[96]. In addition the recent installation of an independent, external x-ray tube for full-field imaging at the Australian Synchrotron^[56], which is orientated perpen-

1
2
3
4
5
6
7
8 370 dicularly to the synchrotron beam, may accelerate the procedure and overcome
9 the impractical translation of the target between imaging and treatment.

10 The first alignment protocol for large animals was developed for ID17 at the
11 ESRF by Donzelli et al.^[97]. The protocol was based on individual treatment
12 planning where the target and the beam directions were defined on a CT image
13 375 with the help of a commercial treatment planning platform. The alignment of
14 the target used fiducial markers as reference points, which were placed on the
15 animal during CT-imaging. Before the treatment, x-ray projection images of
16 the animal on the treatment stage were acquired from different angles. With
17 the aid of manually identified fiducial markers in these projection images, an
18 380 algorithm calculated the correct translation in 3 dimensions and rotation about
19 3 axes to be applied to have the beam orientation as defined in the treatment
20 plan. This protocol was used successfully to irradiate small pigs at ID17 in
21 February 2017.

23 2.7 Organ motion

24
25 385 Organ motion during irradiation can have a serious impact on microbeam dose
26 distributions. The impact of dose blurring has been assessed with MC studies
27 by Donzelli^[98] and Machado de Sola et al.^[99]. Beyond blurring, organ motion
28 is also hazard when aligning microbeam arrays applied from different directions.

29 Organ motion introduces considerable risk of misalignment, particularly for
30 390 interlaced microbeam patterns. Donzelli et al.^[100] introduced a concept called
31 spiralMRT, a geometry offering similar spatial fractionation properties as in-
32 terlaced MRT, while being less vulnerable to target positioning uncertainties.
33 The dose distributions achievable with spiralMRT in a simplified human head
34 geometry were calculated with Monte Carlo simulations based on Geant4 and
35 395 the dependence of the result on the microbeam pitch, total radiation field size,
36 and photon energy were analysed. A comparison with interlaced MRT and
37 conventional MeV tomotherapy was carried out.

38 SpiralMRT delivers homogeneous dose distributions to the target, while us-
39 ing spatially fractionated entrance beams. The valley dose of spiralMRT en-
40 400 trance beams is by up to 40 % lower than the corresponding tomotherapy dose.
41 SpiralMRT thus offers to be a promising approach to delivering homogeneous
42 dose distributions with spatially fractionated entrance beams, possibly decreas-
43 ing normal tissue side effects in hypofractionated radiation therapy.

45 3 Dosimetry

46
47
48 405 Experimental dosimetry is an essential ingredient, together with state-of-the-
49 art dose calculations, for the development and validation of the TPS. The main
50 challenges in MRT dosimetry are on one hand to determine the very high dose
51 rates in the homogeneous field on an absolute scale, taking into account the
52 necessary corrections to be applied for the typical spectrum from a synchrotron
53 410 radiation x-ray source, and on the other hand the dose measurement of an array
54 of x-ray micro-beams, modulated on a micrometer scale.

55 Regarding absolute dose determination in a homogeneous field, ion chambers
56 (section 3.1) are the accepted primary standard, while Alanine-based dosimetry
57 (section 3.2) has obtained increased attention over the past years. This reference
58
59
60

dosimetry is performed prior to the spatial fractionation of the x-ray beam, and Monte Carlo methods are used to convert the reference dose to the dose within the micro-beam field.

For micro-scale dosimetry (MSD), i.e. the determination of the absorbed dose with micrometer spatial resolution, commercially available Gafchromic[®] films are widely utilised, though there are certain limitations as will be detailed in section 3.3. This research has triggered several other developments in experimental MSD. During the last decade several detectors were tested for potential applications in MRT: MOSFET edge-on and silicon strip detectors (section 3.4), high-resolution thermoluminescent dosimeter (TLD, section 3.5), polymer gels^[101–103], Optical Computed Tomography (CT) using a radiochromic plastic named PRESAGE^[104], Fluorescent Nuclear Track Detectors (FNTD) (section 3.6), and optical fiber dosimetry (section 3.7). Most recently, the emergence of commercial, and clinically traceable diamond detectors with micron-scale spatial resolution have appeared on the market and are emerging as potential candidates for MRT dosimetry (section 3.8).

All of the above dosimetry technologies have specific strengths and weaknesses for the very demanding MRT dosimetry requirements. The Gafchromic[®] films, silicon detectors, TLDs, FNTDs and diamond detectors seem currently the most adequate and practical dosimeters. All are described in some detail below. Important for the application of microbeams is the determination of output or scatter factors that relate the dose rate in the homogeneous radiation field with the dose rate in the microbeam peaks. These factors are either determined by dosimetry or with Monte Carlo simulations and are a prerequisite for the precise dosage of MRT.

3.1 Ion chambers

Ionization chambers are the dosimetry standard tool in RT protocols for absolute dosimetry^[105,106]. The validation of a treatment planning system (TPS) is usually done with ionization chamber measurements in a liquid water or solid water phantom. A protocol for absolute dose measurements was put in place for MRT preclinical work^[107]. It is based on the International Atomic Energy Agency's TRS 398 absorbed dose-to-water protocol^[107,108].

Reference dosimetry was performed with the PinPoint 31014 IC (sensitive volume of 0.015 cm³) from PTW for a homogeneous field of 2 cm × 2 cm size and at a depth of 2 cm in a water tank.

The absolute dose in water under reference conditions is given by Andreo et al.^[108]:

$$D_{w,Q} = M_Q \times N_{D,w,Q_0} \times k_{Q,Q_0} \quad (1)$$

where M_Q is the raw reading from the IC corrected for the influence of the temperature and pressure, the polarization between the IC electrodes, the calibration of the electrometer and the ion recombination. Pressure and temperature have to be measured during dosimetry measurement. N_{D,w,Q_0} is the calibration factor for the beam quality Q_0 and k_{Q,Q_0} a factor that corrects for the difference between the beam quality Q_0 used for the calibration and the beam quality Q under which the measurements are performed.

3.2 Alanine dosimeters

Alanine, an amino acid (2-Aminopropanoic acid) is the sensitive material in alanine dosimeters. There are several types of alanine: L or S (+)-alanine, D or R (-)-alanine, beta-alanine etc., but for dosimetry α -Alanine is used ($C_3H_7NO_2$). A stable alkyl free radical $CH_3C\bullet HCOO^-$ is produced upon irradiation. The exposure of an amino acid to ionizing radiation causes the production of radicals of which the number of unpaired electrons is proportional to the absorbed dose over a wide dose range and can be measured by Electron Spin Resonance (ESR) spectroscopy^[109,110]. The measured signal is linear from approximately 2 Gy to 200 kGy. Though Alanine dosimetry is not recognised as a primary RT standard, it is widely accepted as secondary standard for absolute dose measurements^[111,112]. A recent comparative study between PinPoint IC and alanine dosimetry for homogeneous fields revealed an overall agreement between the two methods for a delivered dose between 50 and 5000 Gy of better than 0.7%. The overall uncertainties of the alanine dose measurements were 3.08% and 2.80% at 2σ for alanine analysis with an EMX EPR spectrometer and an e-scan benchtop spectrometer, respectively^[113].

3.3 Radiochromic film dosimetry

Radiochromic films are a common tool in modern radiation therapy dosimetry. Using films, it is possible to measure 2-dimensional dose distributions with sub-millimetric resolution, a fundamental part of treatment plan verification.

The core of the radiochromic dosimeter is a crystalline polyacetylene material responsible for a dose dependent change in optical density. Radiochromic films do not require any chemical treatment, have a weak energy dependence from keV to MeV energies, are dose rate independent and provide spatial resolution between 5 and 25 μm depending on the film type. Film dosimetry is a relative dosimetry method and films are usually calibrated with ionisation chambers under reference conditions.

In conventional RT, the dose variation of the radiation field occurs on a millimetric scale and the film analysis can be performed with a flatbed scanner, providing the required sub-millimetric resolution. The analysis of film irradiated with 50 μm wide microbeams requires a more powerful instrument. Protocols for radiochromic film read-out at the micrometer scale initially used microdensitometers^[80,114,115]. The use of a microscope was suggested in 2009 by N. Nariyama et al.^[116] and since then, developed protocols use an inverted optical microscope^[117].

Microscopes equipped with motorized stages able to move with sub-micrometric precision combined with a charge-coupled device (CCD) camera, allow the acquisition of film areas up to 10 cm^2 in a few minutes with micrometric resolution and the evaluation of unusual field configurations such as pencil beams^[26] or phantoms under motion conditions. Dedicated image processing protocols are being developed to correct the acquired digital images for noise and film inhomogeneities at the micrometric scale^[117,118]. An example of a digitalized film image is reported in Figure 5. From the film analysis, dose profiles are obtained with a reproducibility of 1% and read-out uncertainties of less than 5%.

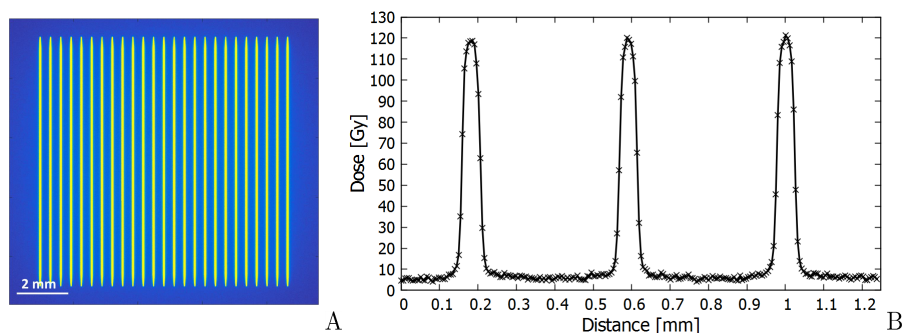


Figure 5: Digital image acquired with an optical inverted microscope of a HD-V2 Gafchromic[®] film irradiated with a 10 mm \times 10 mm field of microbeams (A). Dose profile of 50 μ m wide and 400 μ m pitch microbeams (B).

505 3.4 Silicon Detectors

Radiation dosimetry in conformal radiotherapy using silicon diodes is well documented in the literature and accepted in the clinical medical physics field. The physical parameters of the MRT beams, however, make it impossible to use such commercial silicon diodes for dosimetry. MOSFET detectors provide a high spatial resolution because of their very small radiation sensitive area defined by the thickness of the MOSFET gate oxide layer. Edge-on MOSFET dosimetry is a technique whereby a MOSFET radiation detector is positioned such that its smallest dimension is normal to the incident beam^[119].

At the ESRF profiles of a 30 μ m wide microbeam were successfully acquired using the detector^[119]. The MOSFET detector was also used for measuring the peak and valley doses^[120]. In 2009, the study carried out by Siegbahn et al.^[121] reported PVDRs obtained by MC simulations up to 50 % higher than the experimental PVDR measured with a MOSFET detector. These discrepancies were mainly attributed to the energy dependence of the detector assuming that there was a significant difference between the photon spectrum in the MRT peak compared to the valley. The MOSFET energy dependence was also highlighted in various articles^[122–124].

A silicon single-strip detector (SSD) and associated readout electronics have been developed to allow for very high spatial resolution measurements of the instantaneous dose rate at the detector's position in a phantom^[125–127] (see figure 6). The SSD response can then be integrated to deduce the total absorbed dose. The dynamic range of the readout system is over five orders of magnitude, which is ideal for MRT dosimetry.

The SSD design is also suitable for MRT dosimetry where the intrinsic beam height is usually 500 μ m and microbeam width is typically 50 μ m. The single strip active pad area has dimensions of 250 μ m to 900 μ m long and 10 μ m wide. The SSD is fabricated using ion implantation production techniques. The active layer is a 100 Ω – cm p-type epitaxial layer that is 50 μ m thick and grown on top of the 370 μ m thick silicon substrate of resistivity (0.001 Ω cm)^[126,127].

In recent applications the SSD has been operated in passive mode where the spatial resolution is close to 20 μ m in face-on mode. For the read out, a standard clinical electrometer can also be used. In this way, measurements can

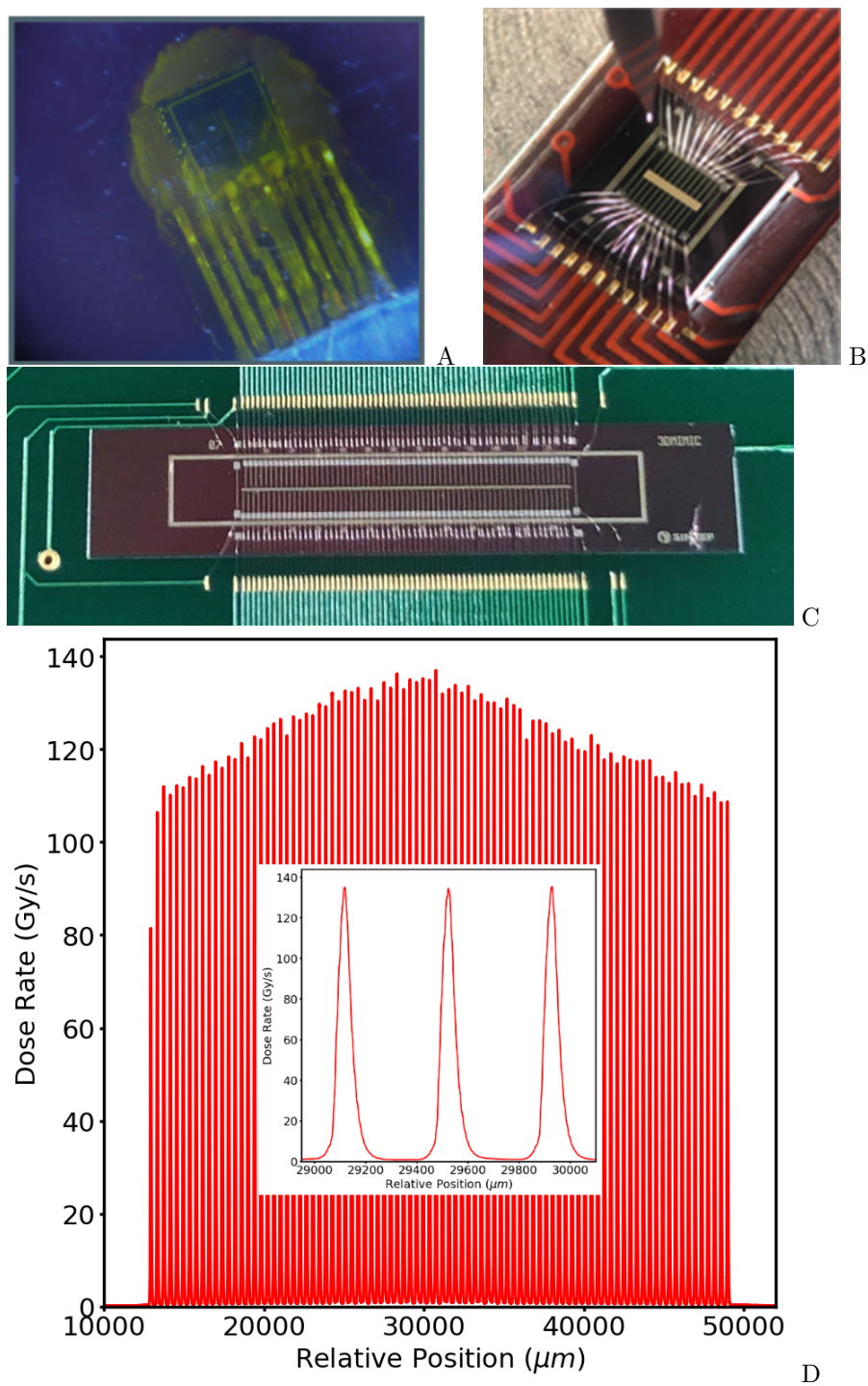


Figure 6: Generations of detectors developed for MRT dosimetry and QA. A: Single silicon strip detector (SSD); B: Multi-strip silicon detector array (20 strips); C: Back-etched transmission silicon detector array (256 strip) for MRT QA; D: Typical 35 mm wide MRT treatment field map measured at the Australian Synchrotron by the SSD with a zoom of 3 microbeams overlaid.

1
2
3
4
5
6
7
8 be more directly compared with other high resolution and clinically relevant
9 dosimeters, under similar irradiation conditions (e.g. ionization chambers in
10 broad beam conditions and other solid state detectors in microbeam conditions).
11 Similar to the MOSFET devices, the best spatial resolution of the SSD of 5 μm
12 is achievable when it is operated in passive mode, edge-on configuration and in
13 good alignment with the microbeams^[107,128]. The combination of the SSD with
14 the fast readout capability of the X-Tream dosimetry system and wide dynamic
15 range allows for precise assessment of the MRT multislit collimator alignment to
16 ensure the accurate reproducibility of the MRT irradiation field and associated
17 dose delivery (see figure 6)^[129].
18

19 3.5 Thermoluminescence dosimetry

20
21 A two-dimensional (2-D) thermoluminescence (TL) dosimetry system consist-
22 ing of $\text{LiF} : \text{Mg}, \text{Cu}, \text{P}$ (MCP-N)-based TL foils and a TLD reader equipped
23 with a CCD camera and the large size (72 mm in diameter) planchete heater
24 was developed at the Institute of Nuclear Physics to perform high resolution
25 dosimetry. TLDs have been used for MRT dosimetry; measured dose distribu-
26 tions were compared with Monte Carlo simulations. Measurements confirmed
27 the findings obtained with Gafchromic films, particularly of a measured valley
28 dose of 10-40 % higher than the Monte Carlo predicted dose^[130].
29

30 3.6 Fluorescent Nuclear Track Detectors

31
32 Fluorescent Nuclear Track Detectors (FNTD) are a new type of luminescent
33 detectors for different applications in radiation dosimetry. They were originally
34 developed for neutron and heavy charge particle dosimetry^[131] and combine the
35 advantages of solid state track detectors and optical measurements without the
36 need for long chemical etching. The detectors are made of fluorescent aluminum
37 oxide single crystals (sapphire) doped with carbon and magnesium ($\text{Al}_2\text{O}_3 : \text{C}, \text{Mg}$).
38 The tracks of secondary electrons generated by the MRT beams in
39 the single crystal aluminum oxide detector are imaged using a high resolution
40 readout system based on confocal laser scanning fluorescence microscopy^[131].
41

42 FNTDs were optimized for imaging applications over 4 orders of magnitude
43 of photon doses^[132] ranging from 5 mGy to 50 Gy and extremely high spatial
44 resolution of 0.6 μm . High spatial resolution and wide dynamic range of dose
45 measurements make FNTD technology very attractive for MRT quality assurance
46 application with a large PVDR^[133]. FNTD is a passive integrating type of
47 detector that does not require wires, electronics or batteries during irradiation.
48 This detector is immune to electromagnetic interference and can measure doses
49 at very high dose rate; it was successfully tested at 108 Gy/s. FNTD detectors
50 provide extremely good temperature and environmental stability, no light sensi-
51 tivity, thermal fading or signal build-up. FNTD imaging plates are reusable
52 after thermal annealing or optical bleaching. The most recent results obtained
53 for MRT are summarized in Bartz et al.^[133].
54

55 3.7 Fiber Optical Dosimeters

56
57 Fiber Optic Dosimeters (FODs) have a significant advantage over many dosime-
58 ters developed for MRT in that they are made of plastic scintillators. In an x-ray
59
60

1
2
3
4
5
6
7
8 radiation field environment their water equivalence makes them excellent can-
9 didates for MRT and worthy of research and development. FODs typically find
10 use in applications where high spatial resolution ($<500\ \mu\text{m}$) is not essential since
11 585 machining to very small thicknesses is very challenging and plastic scintillators
12 have a low light yield (typically tens of thousands of photons per MeV of en-
13 ergy deposited). The synchrotron light source used in MRT can easily provide
14 the necessary x-ray photon flux to facilitate a measurable response in FODs.
15 However, Cherenkov radiation generation, radioluminescence, radiation hard-
16 590 ness and dose rate dependence of FODs requires careful consideration if they
17 are to be used regularly for MRT dosimetry.

18
19 Optical detectors have been applied to imaging microbeam x-rays in the
20 past^[134,135], however, they have not been used at highly brilliant synchrotron
21 light sources. Archer et al.^[136,137] have demonstrated a FOD probe devel-
22 595 opment technique with improved spatial resolution using scintillators and have
23 tested them in an MRT synchrotron x-ray beam, delivering very high dose rates.
24 The scintillator thickness defines the one-dimensional spatial resolution of the
25 FOD probe in the axial direction if it is operated in edge-on mode with respect
26 to the direction and plane of the microbeams. The FOD length is 1 mm in the
27 600 radial direction as determined by the optical fiber core diameter. The scintil-
28 lation light generated in the plastic scintillator is transported along an optical
29 fiber to a photomultiplier tube or silicon photomultiplier.

30
31 The most recently developed FOD has a one-dimensional spatial resolution of
32 10 μm . The detector is able to resolve the individual microbeams, and measure
33 605 the peak-to-valley dose ratio that is consistent with other high spatial resolution
34 detectors under the same irradiation conditions. The role of radioluminescence
35 in the optical fibre used to transport the scintillation photons has been shown
36 to create a significant contribution to the total light detected^[138].

3.8 Diamond Detectors

40
41
42
43 610 Recently a solid state diamond detector, potentially suitable for use as a dosime-
44 ter in MRT, have become commercially available^[139-141]. The PTW model
45 60019 “microDiamondTM” (PTW-Freiburg GmbH, Freiburg, Germany) has a
46 cylindrical active volume of 1.1 mm radius and 1 μm length. The microDiamondTM is
47 a synthetic single crystal diamond detector incorporating Schottky contacts, and
48 615 is designed to be operated in passive mode with an electrometer^[142].

49
50 Operation within the extreme radiation environment (very steep dose gra-
51 dients, high dose rate, kilovoltage energy spectrum) typically used in MRT is
52 well outside the conditions of use recommended by the manufacturer. However,
53 excellent results have been demonstrated, particularly in the penumbra regions
54 620 of the microbeams^[139]. Very careful and precise alignment of the microdiamond
55 is required to achieve such results. The device should be operated in edge-on
56 mode to utilize the 1 μm thick active layer so as to fully exploit the best spatial
57 resolution possible with this device.

4 Dose calculation and treatment planning

4.1 Physics of dose absorption in microbeam radiation therapy

Dose calculation and its validation by experimental data can be performed with high accuracy in conventional RT. Relative dose uncertainties in conventional RT are usually below 3%^[143,144] and dose validation is part of international standards^[145]. In MRT, compliance with such high standards is challenging. The small sizes of the radiation fields, large differences between peak and valley doses and the low photon energies place extraordinary high demands on dose calculation and dosimetry. In this section we present various approaches and physical prerequisites for dose calculations in MRT.

MRT typically uses polychromatic x-ray beams with photon energies at around 100 keV. At these energies photons interact via photoelectric absorption, Compton and Rayleigh scattering. Compton scattering is the most frequent photon interaction. Whereas MeV photons transfer the bulk part of their energy into kinetic energy of secondary electrons, the energy transfer at low photon energy is rather low between 5 and 20%. Therefore multiple photon scattering substantially contributes to the scatter dose. Photoelectric absorption transfers almost all of the photon energy into kinetic energy of a secondary electron. The absorption coefficient of the photoelectric interaction strongly increases with decreasing photon energy and is particularly important for materials with atoms of higher atomic numbers.

Secondary electrons generated in photon interactions of primary, i.e. unscattered photons deposit their kinetic energy predominantly within the microbeam peak regions, due to short electron ranges. The dose in the valley is caused by electrons of primary photons scattering out of the peak region and electrons generated in interactions of scattered photons. If the spacing between microbeams is sufficiently high, i.e. higher than the typical electron range, the PVDR is closely proportional to the ratio of peak width to peak pitch^[79,146]

The absorption coefficient of 100 keV photons is around 5 times higher than for 5 MeV photons. Hence depth dose curves are considerably steeper and the range of secondary electrons is much shorter than 1 mm. The build-up effect, which dominates the first centimeters of conventional MeV-photon RT depth dose curves affects 1 mm or less of the depth dose curves for 100 keV photon beams.

The choice of appropriate photon energies in MRT needs to balance between short electron ranges guaranteeing sharp beam penumbras and shallower depth dose curves allowing to irradiate deeper targets without an excess of surface dose. A shift of the photon spectrum to higher photon energies in a broad wiggler spectrum is usually achieved by adding additional filters. However, these filters also reduce the dose rate. The electron range does not gradually increase with photon energy but depends on the ratio between Compton and photoelectric effect. Since Compton electrons receive only part of the initial photon energy, their range is much shorter than that of photo electrons. Therefore beam penumbras decrease with increasing energies below and increase again above 100 keV photon energy. At 200 keV the Compton electron range reaches 25 μm . A further increase of photo energy leads to a reduction of peak dose and PVDR of 50 μm wide beams. While photon energy is less relevant in small

1
2
3
4
5
6
7
8 animal studies, future clinical applications may require slightly higher photon
9 energies between 150 and 200 keV.

10 11 4.2 Monte Carlo dose calculation

12
13 675 In the past, the majority of MRT dose calculations were performed with Monte
14 Carlo techniques. Early dose estimates involved homogeneous and simplified
15 phantoms and in parts mono-energetic photon beams^[147]. A wide range of dif-
16 ferent Monte Carlo codes has been used for dose calculations. First dose calcu-
17 lations were performed by Slatkin et al.^[29] using an early EGS4 (INHOM)^[148]
18 680 version that includes transport of photons, electrons and delta-rays. However,
19 only total ionization cross-sections were used in the electron transport ignoring
20 the distribution of scattering angles and energies. Simulations in later EGS4 ver-
21 sions^[123,149,150] showed substantial deviations to these early calculations. Later
22 Monte Carlo calculations used the PENELOPE framework^[80,151], a GEANT3
23 PSI-version^[147], GEANT4^[78,81,152] and EGS5^[146]. De Felici et al.^[153] per-
24 685 formed a comparison of different Monte Carlo codes and did not find differ-
25 ences in the dose distributions calculated with GEANT4, EGS4, EGS-NRC
26 and PENELOPE. Due to flexibility and accuracy, Monte Carlo techniques have
27 become the standard in MRT dose calculation.

28 690 Important parameters for precise Monte Carlo simulations are energy cut-off
29 values for electron tracking and the choice of scattering cross section libraries.
30 Particularly at low photon energies the shape of microbeam penumbras and the
31 valley dose depend on the choice of physical models^[154]. When working with
32 synchrotron radiation, the chosen physics libraries should account for polariza-
33 695 tion effects. At the spatial scales of several micrometres condensed history sim-
34 ulations of the electron scattering are sufficient. Only at smaller volumes track
35 structure simulations with tools such as GEANT4-DNA become necessary^[155].

36 Small voxel sizes are a challenge for Monte Carlo simulations. The proba-
37 bility that a voxel is hit by a particle is proportional to its volume. In order
38 700 to keep the statistical uncertainty constant the number of particle histories
39 needs to be scaled inversely proportional to the voxel volume. In contrast to
40 conventional RT, where voxel sizes of approximately 1 mm are sufficient, a mul-
41 tiport MRT treatment may need around 5 μm resolution in all spatial dimen-
42 sions. This would require $8 \cdot 10^6$ times more particle histories and also memory
43 705 than for Monte Carlo dose calculations in conventional radiotherapy. Therefore
44 straight forward Monte Carlo simulations will not be feasible for MRT in the
45 near future and strategies to overcome these challenges have to be provided.
46 The majority of MRT dose calculations were performed for unilateral exposures
47 and hence the voxel size can be reduced in only one spatial dimension^[80,156].
48 710 Other approaches use larger binning sizes and score peak and valley doses sepa-
49 rately^[79,146,157], because anatomical information in a planning CT are provided
50 on a coarse millimeter sized grid.

51 52 4.3 Simulation of radiation sources

53 An accurate description of synchrotron beam properties such as phase space and
54 715 spectrum are a prerequisite for accurate dose calculation. Several early Monte
55 carlo studies assumed ideally parallel microbeams with equal beam intensity.
56 Nettelbeck et al.^[158] investigated the influence of beam divergence and the
57
58
59
60

collimator on the simulated microbeams. They realized an increase in penumbral dose of up to 26% due to beam divergence, although differences in the peak and valley centre disappeared. Martínez-Rovira et al.^[80] did a complete simulation of the medical beam line of the ESRF from the wiggler to the multislit collimator and used the phase space for subsequent dose calculations.

Bartzsch et al.^[152] characterized the phase space and showed that a simplified model of the phase space leads to microbeam dose estimates that do not differ measurably from a full phase space simulation. This model assumes parallel beams within the phantom or patient, leakage radiation in the valley regions behind the absorber material with a different spectrum and accounts for a change of flux due to partial shadowing and the lateral profile of the synchrotron beam intensity.

A special feature of synchrotron radiation is its linear polarization which impacts on the Compton and Rayleigh scattering of photons in matter. Since Rayleigh scattering leads only to small angle deviations of photon trajectories and is not creating secondary electrons, polarization will mainly influence dose distribution via Compton interaction. The differential scattering cross section of the Compton effect is given by the Klein-Nishina Formula

$$\frac{d\sigma}{d\Omega} = \frac{1}{4} r_0^2 \frac{E^2}{E_0^2} \left[\frac{E_0}{E} + \frac{E}{E_0} - 2 + 4 \cos^2 \Theta \right], \quad (2)$$

where E and E_0 are the photon energies of incoming and scattered photon, r_0 is the classical electron radius and Θ the angle between the polarization directions of incoming and scattered photon. Photons are preferentially scattered perpendicular to the polarization direction. One of the first investigating the effect of polarization were Orion et al.^[149] using EGS4. Also De Felici et al.^[123] used EGS4 to investigate how polarization effects the PVDR. They used 25 μm wide beams, 200 μm centre-to-centre spacing and 30 mm \times 30 mm fields in a homogeneous water cylinder. Within the accuracy of the Monte Carlo simulations they did not see any polarization effects within the radiation field. Only in the photon scattering outside the microbeam field differences of up to 10% were observable. Hugtenburg et al.^[146], on the other hand, came to the conclusion that polarisation effects are indeed essential for any future MRT treatment planning.

Studying the dose distribution around a pencil beam reveals how polarisation effects the dose distribution in microbeam fields^[152,154]. Polarisation has a substantial impact on the direction of scattered Compton electrons and Compton photons and leads to a dose anisotropy. Photo electrons remain unaffected by photon polarisation and therefore dose absorption within the range of photo electrons is isotropic. As a consequence peak doses are almost unaffected by polarisation. Although the valley dose is dominated by Compton scattered photons, directional preferences level out within the microbeam field and polarisation corrections of the valley dose are between 1% and 3% in the field centre and field edge, respectively^[152]. Only in the scatter dose region outside the microbeam field substantial differences between polarized and unpolarized photons are observable^[123,146,152].

Despite considerable work and effort for precise dose calculations and dosimetry, substantial deviations between calculation and measurement have repeatedly been reported. Usually calculations are overestimating the PVDR and valley doses in measurements are 10 to 20% higher than predicted in simulations. Various effects may cause these deviations. Frequently discussed are

1
2
3
4
5
6
7
8 influences of the multislit collimator. Although scattering from the collimator
9 into the valley seems to be negligible^[152,158] simulations may induce unaccept-
10 able simplifications, such as perfectly plane surfaces. In fact a chemical analysis
11 of the collimator surface of the biomedical beamline at the ESRF revealed sub-
12 770 stantial amounts of surface depositions, in particular copper. The fabrication
13 process of the multislit collimator itself is challenging^[87] and may infer varia-
14 tions in the peak width and peak distances which are not modelled in Monte
15 Carlo simulations.

16 Furthermore Monte Carlo simulations neglect usually the wave nature of the
17 775 particles they track, such as refraction, diffraction and total external reflection.
18 Even hard x-rays have a refractive index which is slightly different to 1. At
19 100 keV this difference is in the order of $3 \cdot 10^{-7}$ ^[159] leading to a critical angle
20 for total external reflection of around 0.8 mrad. Due to the low divergence of the
21 synchrotron beam, this angle is large enough to cause total external reflection
22 780 at the collimator walls even for the outermost beams of a $30 \text{ mm} \times 30 \text{ mm}$ field.
23 Future investigations are required to reveal the cause of remaining discrepancies
24 between simulation and measurement.

25 26 4.4 Alternative dose calculation methods

27 28 4.4.1 Semi-adjoint Monte Carlo simulations

29
30 785 As mentioned in section 4.2, the main problem when applying Monte Carlo
31 tools to MRT are the required small voxel sizes. Monte Carlo problems with
32 small detector volumes or when studying variable sources are often treated in
33 their adjoint form^[160,161]. Mathematically, Monte Carlo simulations can be
34 seen as an integration of the Boltzmann transport equation^[160]. In the adjoint
35 790 version of this integro-differential equation, detector and source term exchange
36 their position. Hence, in the adjoint Monte Carlo simulation all 6 phase space
37 dimensions of detector and source are swapped and interactions are tracked
38 "backwards in time".

39 For MRT, the detector volume is small in the two dimensions perpendicular
40 795 to the beam propagation. The MSC, as photon source has a large phase-space
41 extension perpendicular to the propagation direction, while the source is small
42 in all other phase space dimensions. Therefore the adjoint Monte Carlo problem
43 will not lead to an advantage. However, it is possible to formulate a semi-adjoint
44 version of the Monte Carlo problem exchanging only the two spatial dimensions
45 800 perpendicular to the beam direction (see figure 7). As the momentum dimen-
46 sions of detector and source remain unchanged in the phase space, particles can
47 be tracked "forward in time". However, this partially adjoint version of the
48 Boltzmann transport equation can only be derived if the phase space variables
49 clearly separate, restricting this method to problems which are homogeneous
50 805 perpendicular to the propagation direction and demand material homogeneity.

51 Theoretical derivations of this problem may be found in the respective liter-
52 ature dealing with Monte Carlo techniques and the Boltzmann transport equa-
53 tion. Here we only provide a brief heuristic explanation. Consider a photon
54 emitted from the source element dS in the forward Monte Carlo problem in
55 810 figure 7A. The probability that a certain energy fraction dE of this photon is
56 absorbed in the detector volume element dV_D is equal to the probability that
57 the same energy fraction dE of a photon leaving the semi-adjoint source ele-

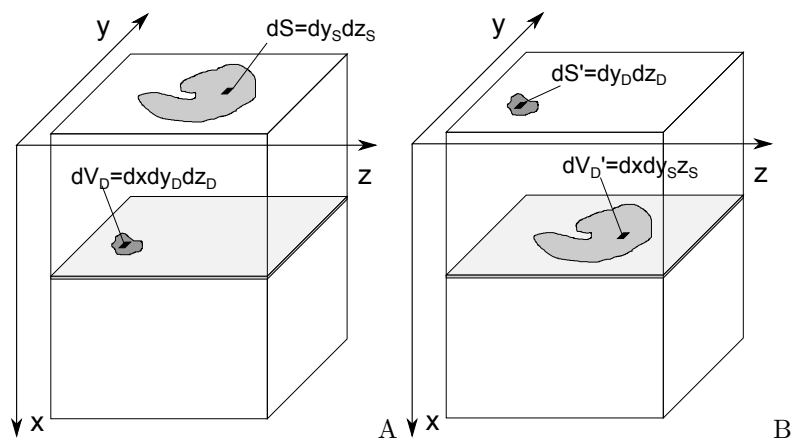


Figure 7: Forward (A) and semi-adjoint (B) Monte Carlo transport. An exchanging of source and detector geometry in the y - z -plane will lead to the same expected energy absorption in the detector, if the number of particles per source area is identical. Prerequisite is the homogeneity of the phantom in the y - z -plane.

ment dS' in figure 7B is absorbed in the semi-adjoint detector element dV_D' . More complicated source and detector geometries can be considered as compositions. If the number of particles emitted per source volume is equal for all source elements, the expectation of energy absorption in the forward detector and semi-adjoint detector will indeed be equal.

This method was employed by various authors^[26,117,146,152]. It is particularly useful to determine so called relative output or scatter factors (ROF). With a single simulation it is possible to calculate ROFs for various field shapes. However, the restriction of this method to slab geometries limits its use in MRT treatment planning.

4.4.2 Kernel based dose calculation approaches and hybrid dose calculation

Despite a wide spread use of kernel based dose calculation algorithms in conventional RT for MeV photons, such algorithms are rarely used in the low energy x-ray domain below 1 MeV. In order to deal with tissue inhomogeneities, existing kernel based algorithms employ O'Connor's electron density scaling method^[162-164], which is not applicable at low photon energies. Nevertheless, kernel based dose calculation methods for lower photon energies^[165-167] and also for MRT^[157,168] have been developed. Such kernel based dose calculation algorithms are capable of calculating microbeam dose distributions within five minutes and further acceleration seems technically feasible^[157]. However, comparisons with Monte Carlo simulations show larger deviations, particularly in the valley regions.

Accurate and fast dose calculation can be achieved by combining kernel based and Monte Carlo based techniques in a hybrid approach. Problematic for kernel based dose calculation is the scattering of photons in inhomogeneous material. On the other hand, the tracking of secondary electrons on a micrometre

1
2
3
4
5
6
7
8 840 scale is time consuming for Monte Carlo calculations. Photon scattering on a
9 millimeter grid can be computed very efficiently, even within a few seconds as
10 demonstrated in the past^[169–171]. Kernel algorithms can calculate the electron
11 scattering with high accuracy assuming homogeneous material. Information on
12 tissue inhomogeneities are given on a coarse millimeter sized grid.

13 845 In a hybrid dose calculation approach, Monte Carlo methods are used to
14 calculate primary and scatter photon dose on a millimeter grid without consid-
15 ering electron scattering. In a subsequent electron convolution algorithm the
16 microbeam pattern is calculated. Donzelli et al.^[79] were able to show that such
17 algorithms are around 600 times faster than pure Monte Carlo simulations and
18 850 that there are no relevant differences in the calculated dose distributions when
19 compared to pure Monte Carlo. Polarization effects and source phase space can
20 be easily integrated into such hybrid methods.

21 22 4.5 Treatment planning

23 MRT treatment planning has to overcome several challenges compared to con-
24 855 ventional RT. The dose needs to be calculated on very small spatial scales. As
25 described above this requires specialized methods in dose calculation, but also
26 storage and visualization of the calculated dose distribution deserves extra con-
27 siderations. Quality assurance criteria such as the Γ index consider absolute
28 dose changes or dose changes relative to the maximum dose^[172]. Since the Val-
29 860 ley doses are only 5% of the peak dose, a valley dose accuracy of only 10%
30 would require a very strict dose accuracy in the Γ -index of only 0.5%. Another
31 challenge is the low photon energy and the related sensitivity to material com-
32 position. This requires special care when converting CT Hounsfield units into
33 material composition for dose calculation.

34 865 Most preclinical studies in MRT used a few summary measures to char-
35 acterize the dose distribution such as peak dose, valley dose or PVDR. Such
36 measures can be calculated and visualized on a conventional millimeter sized
37 grid. The definition of peak and valley dose requires some, often neglected at-
38 tention, though. All dose measurements and calculations provide dose values
39 870 on a finite grid and therefore some form of spatial averaging. However, because
40 the doses vary on very small length scales, peak and valley doses should always
41 be reported together with the applied averaging or voxel sizes for comparison.
42 It would be desirable to establish standards on how peak and valley doses are
43 presented.

44 875 The relevant radio-biological dose measure in MRT is a matter of ongoing
45 research. Early studies in MRT usually used peak dose to compare biological
46 results^[30,40,173,174], since peak dose is the easiest accessible quantity. More
47 recent results show, however, that rather the valley dose is deciding on biological
48 effects^[36,45], tumour control and tissue damage. A typical configuration of a
49 880 microbeam exposure is 50 μm wide beams with a spacing of 400 μm . "Perfect
50 microbeams" with a sufficiently high peak dose and no valley dose, would kill
51 1/8th of the cells in the microbeam peaks and leave 7/8th of the cells in the
52 valleys unaffected. A reduction of cell survival by 1/8th would correspond to
53 only a few cGy homogeneous dose. Hence, the valley dose will mainly determine
54 885 clonogenic cell survival if intercellular communication can be ignored.

55 Under the assumption that the clonogenic cell survival is determining tissue
56 damage or tumour control and that only dose decides upon the fate of a cell,
57
58
59
60

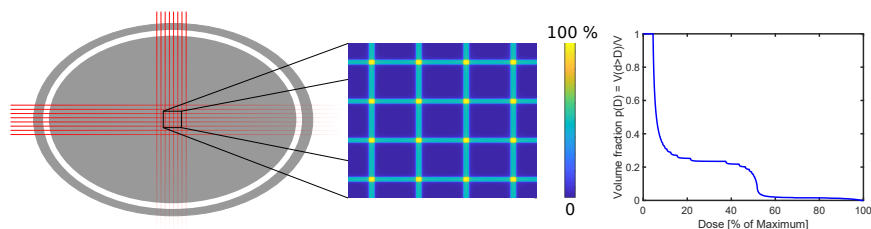


Figure 8: Voxel based dose volume histogram (right) for a cross firing geometry of microbeams (left).

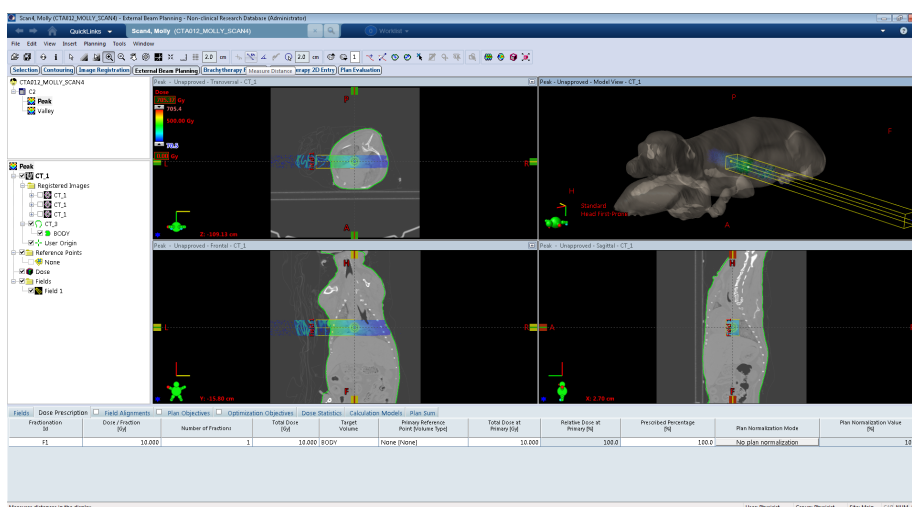


Figure 9: Treatment planning in preparation for pet clinical trials at the Australian Synchrotron with a combination Eclipse and the hybrid dose calculation.

i.e. no bystander mechanisms, the equivalent uniform dose (EUD)^[175] would be the optimal parameter for MRT treatment planning as suggested by Meyer et al.^[176]. The advantage of this measure is its independence of beam geometries. For any microbeam dose pattern, even in cross firing regions the EUD can be calculated upon voxel based dose volume histograms as suggested by Donzelli et al.^[79] (see figure 8).

Dose calculation algorithms have been coupled to TPS as in conventional RT. Such systems allow to define target volumes in CT-images of future patients, the adjustment of beam parameters such as field size, filtering, beam direction, microbeam width and spacing and the visualisation of calculated treatment doses and parameters. The first MRT TPS was based on a PENELOPE Monte Carlo dose calculation engine^[177]. Debus et al.^[157] presented the TPS VIRTUOS^[178] with a kernel based dose calculation engine. Recently a hybrid dose calculation engine has been coupled to the popular TPS Eclipse®(Varian)^[179] (see figure 9).

5 Multimodal MRT

While microbeam radiotherapy produces a unique way of selectively targeting cancerous tissues, further normal tissue sparing or tumour radio-sensitivity enhancement could be achieved with a multimodal approach combining MRT with nanoparticles (NPs) and/or chemotherapies.

The idea that the therapeutic index of MRT could be further improved by combining MRT irradiation with dose enhancers was first proposed by Dilmannian et al.^[180]. Synchrotron MRT beams in the 100 keV range are naturally prone to large absorption cross sections in elements with high atomic numbers, increasing secondary electron production associated mainly with the photoelectric effect. Contrast agents such as iodine, gadolinium or gold were proposed as possible candidates. Monte-Carlo simulated dose enhancement factors for MRT were obtained for different iodine, gadolinium and gold concentrations. A clear superiority was shown for gadolinium and gold with respect to iodine for dose enhancement in a human head phantom geometry^[181]. Other elements like thallium, lutetium or hafnium proved to also give satisfactory enhancements depending on the geometry of the irradiation^[182].

If *in silico* analysis emphasized the interdependent roles of irradiation geometry, synchrotron beam energy and the choice of contrast agent material, the reality of *in vitro* and *in vivo* experiments add extra layers of constraints in the optimization problem. Tumour selectivity and specificity, injection modes and timing, contrast agents' size, micro- and macroscopic distribution, toxicity and retention, all become parameters of critical importance together with the choice of cell lines and animal models. Experimental verification of predicted dose enhancements is however crucial to demonstrate efficiency and better understand the underlying physical, chemical and biological mechanisms of interactions between the synchrotron microbeams and the dose enhancers.

Among other metallic high-Z NPs, gold NPs seem to be privileged candidates for multimodal MRT due to their relatively low intrinsic toxicity, high biocompatibility and their capacity to diffuse and concentrate in tumours. Gokeri et al.^[183] simulated that the hypothetical presence of 7 mg of gold per gram of tumour in a realistic head phantom irradiated with synchrotron microbeams would lead to substantial target dose increase allowing reduced skin, skull bone and maximum brain doses to produce the desired target dose. This dose increase was experimentally evidenced using normoxic polyacrylamide gels and bovine aortic endothelial cells exposed to 1 mMol/L gold NPs^[184]. Interestingly, the gold NPs seem to influence the recovery rate of eradicated area *in vitro*, with a distinct behavior in favor of normal cells compared to cancerous ones which emphasizes once more a differential effect of MRT^[185]. In an *in vivo* experiment, Miladi et al.^[186] showed that gold NPs coated by gadolinium chelates improved survival of synchrotron MRT treated rats bearing intracerebral 9L gliosarcoma (9LGS), an extremely radioresistant tumour.

Among the strong candidates, gadolinium based NPs are currently gaining popularity worldwide with the advances of image guided radiotherapy, in particular MRI guided radiation therapy delivery systems. Beyond their paramagnetic properties, the presence of the high-Z gadolinium atom makes them suitable as radiation dose enhancer. This was evidenced *in vivo* by Le Duc et al.^[187] where rats bearing intracerebral 9LGS had their survival increased by a factor of five when gadolinium NPs were intravenously administered 20

1
2
3
4
5
6
7
8 minutes before their MRT treatment. Le Duc et al.^[188] further demonstrated
9 that more conventional gadolinium chelates did not appear to be of any benefit
10 compared to AGuIX[®], a gadolinium-based NP, that has now reached clinical
11 995 trials with conventional radiation beams. Further optimization of the time se-
12 quence showed the radiosensitizing effect of the gadolinium NPs is increased
13 when MRT is delivered 24 hours after injection, when the tumoral and cellular
14 distributions of the NPs maximize lethal effects^[189].

15 The importance of NPs' cellular distribution, especially in the unique spa-
16 960 tially fractionated dose distributions of synchrotron microbeams, was also em-
17 phasized by Engels et al.^[190] for the specific example of Tantalum pentoxide
18 NPs. These non-toxic, nano-structured ceramic compounds were recently intro-
19 duced as possible radiosensitizer and observed to form shells around cell nuclei
20 instead of distributing homogeneously in the medium, producing remarkably
21 965 different physical dose enhancements. This study showed that NP dose en-
22 hancement for synchrotron MRT is highly dependent on the NP congregation
23 properties, location of congregations with respect to the beam peak, and photon
24 energy.

25 In order to further improve the radiotherapeutic efficacy of MRT, other
26 970 methods were developed by combining the effects of existing or novel anti-cancer
27 drugs. If existing chemotherapy drugs like cisplatin or temozolomide did not
28 significantly improve the lifespan of the MRT treated rats with intracerebral 9L
29 gliosarcoma, synergetic effects were observed *in vivo* using tubulin polymeriza-
30 tion inhibitor JAI-51^[65]. The enhanced radio-sensitization of this antimetabolic
31 975 drug was strongly correlated to G2/M phase cycle arrest. A major contributor
32 to MRT efficacy is the immune response modulation^[50]. Smilowitz et al.^[67]
33 demonstrated that gene-mediated immunotherapy provides an important syn-
34 ergetic effect when combined with MRT, with almost 50 % of the treated rats
35 being long term survivors (>1 year). The preferential action of MRT on vascular
36 980 network also lead to some other intrinsically linked radiation sensitization, im-
37 mune function or chemotherapy efficacy improvement mechanisms, e.g tumour
38 oxygenation, which could be further exploited with anti-angiogenic agents^[191].

39 In a more holistic approach, simultaneous use of chemotherapy drugs and
40 NPs also opens the door to more complex theranostics aimed at image-guided
41 985 and targeted selective lethal damages enhancement. Recent advances in the field
42 of cancer therapy are focused on the design of novel drug delivery systems that
43 feature therapeutic, diagnostic and imaging capabilities simultaneously. MRT
44 will undoubtedly benefit from these advances.

45 46 47 48 49 50 51 52 53 54 55 56 57 58 59 60

6 Novel and future radiation sources

990 One of the main obstacles to the clinical translation of MRT is a lack of compact
microbeam sources. Currently only a few large synchrotrons worldwide seem to
be capable of generating the required beam properties. It is commonly accepted
that the benefit of MRT over conventional RT critically depends on high PVDRs,
low beam penumbras and sufficiently shallow dose fall-off with depth in order
995 to treat deep seated tumours. Only radiation qualities that show little lateral
scattering and generate short-ranged secondary particles are able to meet these
criteria. Photon beams with kinetic energies between 100 keV and 300 keV seem
to offer an acceptable compromise between low lateral scattering and low peak

entrance doses when targeting deep seated tumours. Also proton beams were suggested to be used in MRT. However, due to lateral scattering close to the Bragg-Peak, spatial modulation is lost in the target region.

Apart from an appropriate radiation quality the source needs to provide low divergence and a source dimension which is smaller than the size of the generated beams, to ensure constant beam profiles with distance from the collimator and to keep beam penumbras small. Particularly challenging is the conservation of the micrometre sized dose profiles under the conditions of cardiovascular and respiratory motion in the traversed tissue. Radiation doses have to be applied within fractions of a second. Only a few large third generation synchrotrons are currently able to provide such high dose rates. Donzelli et al.^[192] investigated the effect of cardiovascular brain motion during MRT treatment and came to the conclusion that dose rates of 12.3 kGy s^{-1} are necessary to ensure steep dose penumbras. However, radiobiological evidence for the requirement of such high dose rates is still missing and *in vivo* experiments at lower dose rates have already successfully been carried out.

Third generation synchrotrons are large research facilities, with limited capacity for clinical studies in MRT and they are too expensive to be dedicated to cancer therapy alone. If MRT is to be established as a widespread radiotherapy treatment option, alternative compact microbeam sources need to be developed. Synchrotrons may demonstrate the principle feasibility of MRT, but are unlikely to provide widespread clinical applications.

6.1 Inverse Compton Scattering sources

Promising and frequently discussed alternative radiation sources in MRT are inverse Compton scattering sources such as the Munich compact light source^[193,194]. The principle of inverse Compton scattering is similar to synchrotrons. Instead of periodically deflecting electrons in static magnetic fields of undulators or wigglers, electrons interact with the electric field of a strong laser. Because the wavelength of emitted x-ray photons scales with the period of the wiggler field, lower electron energies are required to generate hard x-rays. The energy E_x of the emitted x-rays is approximately given by^[195]

$$E_x = 4\gamma^2 E_L \quad (3)$$

with a narrow spectrum.

Microbeams have been produced at the Munich Compact Light Source (MuCLS), the first commercially sold inverse Compton scattering source (Lyncean Technologies Inc., USA). The first *in vitro* studies were published^[196] and currently *in vivo* studies in mice are being carried out^[197,198]. MuCLS operates with a 4.6 m circumference storage ring with electrons of up to 45 MeV kinetic energy and produces photon energies between 15 and 35 keV. The source diameter is around $42 \mu\text{m}$. First preclinical *in vitro* experiments used 25 keV photons with a dose rate of 1 Gy/min at 1.7 m distance from the source. Due to the low photon energies a 200 μm thick tungsten foil with 50 μm wide slits was sufficient to collimate microbeams with a pitch of 350 μm ^[196].

The future usability of inverse Compton scattering sources for clinical applications in MRT depends on the possibility to upscale flux and photon energy of current machines. There are currently two designs investigated, linear accelerator based systems, which produce a slightly higher brilliance and storage

Project	Place	Type	E_X (keV)	Flux (ph/s)	Source size (μm)
TTX	Beijing, China	SR	20-80	10^{12}	50
NESTOR	Kharkov, Ukraine	SR	30-500	10^{13}	70
ThomX	Orsay, France	SR	20-90	10^{13}	70
KEK QB	Tsukuba, Japan	Linac	35	10^{13}	10
KEK ERL	Tsukuba, Japan	Linac	67	10^{13}	30
MIT	Cambridge, USA	Linac	3-30	10^{14}	2

Table 1: Inverse Compton scattering source projects with sources that provide more than 10^{12} ph/s. SR stands for storage ring, Linac for linear accelerator. Table adapted from Jacquet and Suortti^[199].

ring based systems, such as MuCLS. Although linear accelerator based system offer a higher brilliance, storage ring based systems seem to be better suited for radiation therapy.

Despite substantial progress in the last years, Jacquet and Suortti^[199] estimate that even for ThomX, one of the most advanced systems being currently developed, the achieved dose rate will be in the order of a few Gy/min at an energy of up to 90 keV for clinically relevant field sizes. Table 1 shows currently developed inverse Compton scattering sources and their parameters.

6.2 Compact x-ray tube based microbeam sources

Conventional x-ray tubes are an abundantly available and inexpensive source of x-rays. In x-ray tubes electrons are accelerated to kinetic energies of up to several hundred keV and hit a target made of materials with high atomic numbers (usually tungsten). Interactions between electrons and target atoms generate bremsstrahlung and characteristic x-ray photons, which are emitted almost isotropically into a large solid angle. The efficiency of the conversion of electron beam energy into x-ray energy is very low in the order of around 1%. Most of the kinetic electron energy is converted into heat. To keep the surface temperature of the target below the melting point, the intensity of the electron beam in the focal spot is limited leading to a trade-off between focal spot (source) size and flux. Typical spot sizes are in the order of a few millimetre. As x-ray tubes deliver a strongly divergent x-ray beam the dose rate is comparably low at reasonable distances from the focal spot. Hence, when using x-ray tubes for MRT, beam divergence close to the source, small relative output factors (ROF) and partial shadowing behind the collimator openings impair the microbeam field.

Several investigators developed compact microbeam systems for preclinical research^[200,201]. However, most of these preclinical systems have larger aperture widths and should therefore rather be classified as minibeam systems. Fabrication of appropriate collimators is one of the most difficult steps in the development of x-ray tube based microbeam irradiators.

Recently, small animal radiotherapy platforms were developed to provide clinical standards in preclinical radiotherapy research, e.g. by establishing image guidance and treatment planning tools^[202]. Such preclinical radiotherapy platforms have recently also been used for the production of microbeams (or minibeams). Prezado et al.^[203] described a SARRP (Xstrahl Ltd, UK) based system with a 30 mm thick brass collimator that produced 400 to 500 μm wide beams with a centre to centre distance of around 1200 μm accounting for beam

1
2
3
4
5
6
7
8
9
10
11
12
13
14
15
16
17
18
19
20
21
22
23
24
25
26
27
28
29
30
31
32
33
34
35
36
37
38
39
40
41
42
43
44
45
46
47
48
49
50
51
52
53
54
55
56
57
58
59
60

divergence. As the dose rate at the isocentre was too low they moved to 20 cm source distance and achieved 3.5 Gy/min with a PVDR of around 12. With such a system they were able to achieve 58 Gy peak dose in a preclinical study with rats. In order to further increase the dose rate, they moved the sample off the isocentre closer to the source. Thus, unfortunately many of the features in the small animal radiotherapy platform are lost.

Esplen et al.^[204] investigate possibilities to produce finer microbeams with 100 to 200 μm width at the SARRP isocentre and also tested a very simple collimator made of steel septa and double sided tape that produces 135 μm wide beams. They estimate the achievable peak dose to be roughly 90 Gy, assuming anesthesia to be limited to 1 h maximum.

A set-up that produces the typical microbeam configurations achieved at synchrotrons was presented by Bartzsch et al.^[46]. The authors used a tungsten collimator with divergent slits and achieved a dose rate of 10-18 Gy/min in only 6 cm distance from the focal spot of a 160 kVp x-ray tube. The PVDR of the 50 μm wide and 400 μm spaced beams was as high as 30, but depended strongly on the distance to the collimator. Due to the large divergence of the produced microbeams, the system was dedicated to *in vitro* research only.

6.3 Advanced x-ray tube technology

6.3.1 Carbon nanotube field emission technology

Schreiber and Chang^[205] investigated carbon nanotube field emission technology (CNT) as a mean to produce microbeams with x-ray tubes. In contrast to conventional thermionic electron emission requiring high cathode temperatures, CNT technology exploits high electric fields close to nanometer sized cathode structures to extract electrons at room temperature. The advantage of CNT cathodes over conventional thermionic cathodes are the achievable high electron current densities and small emittance^[206]. Schreiber and Chang^[205] proposed a ring arrangement of anode segments around the patient as shown in figure 10. The electron beam is shaped to match the size of the projection of the collimator opening on the anode surface. A 10 cm thick single slit collimator with 100 μm slit width produced a single microbeam and by vertical translation between source and target several parallel microbeams can be applied. In Monte Carlo simulations they calculated the dose for a ring assembly of 24 cathode segments and estimated that such an assembly could deliver up to 280 Gy/s. Due to the ring geometry the entrance dose can be substantially reduced and reaches only 10% of the target dose. Moreover, they showed that a reduction of photon energy from 225 kVp to only 100 kVp has only minimal impact on the dose in the isocentre.

Hadsell et al.^[93] presented a first prototype of a system with a 0.14 mm wide and 162 mm long focal track. With an acceleration voltage of 160 kV, 70 mA anode current they achieved a dose rate of 2 Gy/s in pulses of 0.1 s. A collimator produces a 300 μm wide beam. They apply these beams with 900 μm centre-to-centre spacing in a mouse experiment by shifting the sample holder and achieved 13 Gy peak entrance dose with a PVDR of 17. In another study they also demonstrate the feasibility of the ring shaped set-up^[47], although at much lower photon energy and dose rate.

However, until now there is no clinical system available and the microbeam

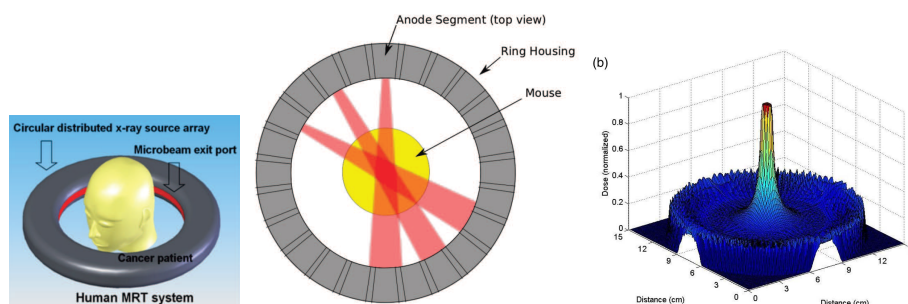


Figure 10: Ring geometry of carbon nanotube field emission technology x-ray tube developed by Schreiber and Chang^[205]. The distribution of the source allows to create high peak doses in the isocentre while keeping the peak entrance dose low. Figure from^[205]

1130 width is rather in the minibeam domain. Whether such broader beams provide
 1135 the same medical benefit as thinner beams needs to be validated. Moreover,
 1140 the application of larger field in human sized targets may lead to substantially
 1145 reduced PVDRs.

6.3.2 Line focus x-ray tube

1135 Another recently developed concept is termed line focus x-ray tube^[46]. This
 1140 concept suggests similarly a strongly eccentric focal spot on a rapidly rotating
 1145 target. Monte Carlo simulations showed that such a system could provide a
 1150 dose rate of 180 Gy/s in 0.5 m distance from the focal spot. At very high target
 surface velocities and high acceleration voltages, electron scattering is the dominant
 energy transport in the target instead of heat conduction. Consequently, heat
 capacity alone decides upon the focal spot temperature and a change in the focal
 spot width does not influence its temperature. Hence the focal spot width is only
 limited by lateral scattering of the electrons.

Due to the small focal spot width the ROF becomes approximately 1. For a
 clinical system, Bartzsch et al.^[46] suggested an acceleration voltage of 600 kV
 at a power of 1.5 MW. The maximum pulse length was estimated to be around
 4 s delivering more than 700 Gy peak entrance dose. The higher mean photon
 energy of 150 keV will be advantageous for patient treatment due to a higher
 penetration depth. However, an experimental proof of concept remains out-
 standing.

6.4 Proton microbeams

1155 Although research in MRT has primarily focused on photons, also particles
 have been investigated as a source for microbeams. Dilmanian and Meek^[207]
 proposed to use heavy ions for MRT but excluded protons from their patent,
 because they show strong lateral scattering. Nevertheless, particularly protons
 have recently gained attention, as proton beams are relatively easy to produce
 and shape. With depth these proton microbeams widen and the spatial dose
 modulation is lost in the Bragg peak region. In practice tissue sparing by dose
 modulation is achieved in the beam entrance region, whereas the tumour is

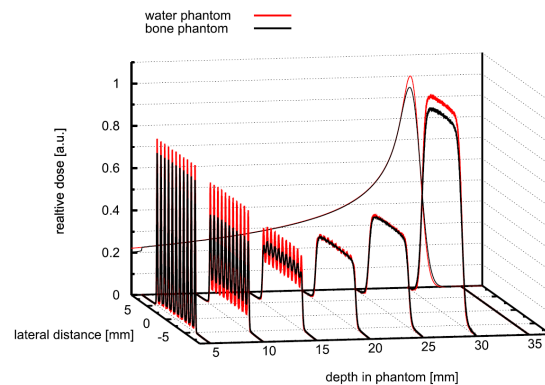


Figure 11: Simulated dose distribution of 60 MeV proton microbeams with $100\ \mu\text{m}$ width and 1 mm spacing; Kłodowska et al.^[208]. The phantom was either a homogeneous water cylinder (red) or a water cylinder with a bone slab (black). Dose distributions are normalised to their maximum. The background shows the mean depth dose curve.

1160 treated with a conventional homogeneous dose as shown in figure 11. Hence, the
 1161 technique is very similar to conventional proton therapy but with an additional
 1162 normal tissue sparing effect in the beam entrance region.

1163 Zlobinskaya et al.^[209] were the first to introduce spatially fractionated radi-
 1164 ation therapy with protons and proposed so called micro-channels: 10 to $50\ \mu\text{m}$
 1165 wide pencil beams irradiated in a two dimensional grid with $500\ \mu\text{m}$ spacing.
 1166 Preclinical studies have shown that proton micro-channels lead to a similar tis-
 1167 sue sparing effect as photon microbeams^[27].

1168 Two methods were pursued to shape proton microbeams, spot scanning^[208]
 1169 and beam collimation by absorbers^[210]. For the spot scanning technique con-
 1170 ventionally proton facilities with active beam shaping systems could be used if
 1171 the longitudinal and transversal brightness of the proton beams is increased,
 1172 which is technically difficult. The technically simpler passive beam shaping
 1173 comes at the cost of contaminating the radiation field with neutrons.

1174 Prezado and Fois^[210] investigated the possibility to use high energy protons
 1175 of 1 GeV for the production of microbeams or minibeam. Since the range
 1176 of 1 GeV protons is substantially larger than the size of a patient, the spatial
 1177 modulation is preserved throughout the patient. However, currently only the
 1178 Petersburg Nuclear Physics Institute, Russia, operates a synchrocyclotron ca-
 1179 pable of producing 1 GeV protons for medical applications. It is questionable
 1180 whether laser accelerated particle sources will ever be compact and powerful
 1181 enough to provide a reasonable alternative.

7 Conclusions

1182 Access to suitable synchrotron light sources has limited MRT research to a small
 1183 research community and has complicated the process of clinical translation until
 1184 now. However, over time, a wealth of pre-clinical data has been acquired that
 1185 impressively demonstrates the efficacy of microbeams in cancer treatment and

1
2
3
4
5
6
7
8 also in neurological disorders such as epilepsy. The safe and responsible treat-
9 ment of patients with microbeams requires solutions to several technological and
10 medical physics challenges in MRT which are related to: the micrometre scale
11 1190 and gradient of the beams, the extremely high dose rates at synchrotrons, the
12 low photon energy, and the development of compact alternative x-ray sources.
13 This article reviewed these challenges and existing solutions. Despite these chal-
14 lenges, powerful dosimetry and dose calculation tools have been developed for
15 MRT and are ready to use for first veterinary and human applications.

16 1195 The need for treatment planning of micrometre sized radiation fields has led
17 to the development of a range of dose calculation methods reviewed in chapter 4.
18 Although Monte Carlo simulations are the standard for MRT dose calculation,
19 the spatial dimensions required to score radiation doses render straight forward
20 Monte Carlo solutions impractical for clinical applications. Appropriate scoring
21 1200 methods can reduce the number of required particle histories and curtail the
22 amount of data. There exist also some alternative approaches to Monte Carlo
23 techniques; particularly hybrid methods combining accurate Monte Carlo tools
24 with fast convolution algorithms seem attractive.

25 A matter of debate is the clinically relevant radiation quantity that should
26 1205 be used for treatment planning, e.g. peak dose, valley dose or integrated dose.
27 A promising approach may be the equivalent uniform dose (EUD) which re-
28 lates inhomogeneous dose distributions to a homogeneous dose that would lead
29 to equivalent cell survival. A final solution to this question requires further
30 preclinical data and radiobiological models.

31 1210 The high dose rate at synchrotrons poses a safety risk for patients, which
32 needs to be handled reliably. Interlock systems and beam switches need to oper-
33 ate at high speed. At the European Synchrotron a patient safety system (PASS)
34 was developed combining monitoring and shutter systems to handle these risks.
35 To keep microbeam penumbras sharp, low photon energies of around 100 keV
36 1215 are used in MRT. The downside of such low photon energies are steep dose fall-
37 offs with depth, known from early days of radiotherapy and treatments with
38 orthovoltage radiation. A possible solution to this problem may be a concomi-
39 tant treatment with dose enhancers such as gold or gadolinium nanoparticles,
40 discussed in section 5. For treatment of patients the chosen photon energy spec-
41 1220 trum needs to be a compromise between sharp beam penumbras and reasonable
42 penetration depth.

43 Synchrotrons are likely to be the first place for clinical trials in MRT. Cur-
44 rently, the Australian and the European Synchrotron are investing in veterinary
45 MRT trials as an intermediate step towards clinical applications in human pa-
46 1225 tients. The purpose of veterinary trials – treating pet animals suffering from
47 spontaneously growing tumours – is two-fold. Firstly, essential radiobiological
48 data will be collected for both normal tissue toxicity and tumour control on a
49 scale more closely resembling humans. Secondly, technological advancements,
50 including treatment planning, image-guidance and patient positioning systems,
51 1230 will be tested, validated and refined for future clinical use.

52 In the long-term, clinical trials at large, synchrotron research facilities are lo-
53 gistically demanding. The widespread clinical use of MRT at synchrotrons is un-
54 likely, although not impossible. Several promising alternative sources are under
55 development and are already used for pre-clinical research. In the future, such
56 1235 sources could provide clinically suitable microbeams in a conventional hospital
57 environment and convert MRT from an experimental method into a routinely
58
59
60

1
2
3
4
5
6
7
8 deliverable treatment option. Furthest progressed are x-ray tube based concepts
9 such as carbon nanotube cathode technology and line focus x-ray tubes, as they
10 achieve dose rates of more than 100 Gy/s with appropriate photon energies.

11 1240 To conclude, the promising therapeutic features of MRT are intrinsically
12 tied to its distinct and demanding physical properties. The field of MRT has
13 a clear clinical trajectory, however, the fulfilment of this pathway largely relies
14 on advancements in medical physics. Although challenges undoubtedly remain,
15 significant and encouraging progress has been made. With the continued develop-
16 1245 opment of suitable solutions for the challenging physics of x-ray microbeams,
17 the first veterinary and human trials of MRT are within reach.

18 19 **8 Acknowledgement**

20
21 We dedicate this review article to the memory of Dr Elke Bräuer-Krisch (BE,
22 PhD) who sadly passed away on 10 September 2018.

23 1250 Elke was a central figure in Synchrotron MRT research and was known
24 around the world for her outstanding contributions to the field, in particular
25 MRT dosimetry.
26
27

28 **References**

- 29
30 [1] Darren Hargrave, Ute Bartels, and Eric Bouffet. Diffuse brainstem glioma
31 1255 in children: critical review of clinical trials. *The lancet oncology*, 7(3):241–
32 248, 2006.
- 33 [2] Rebecca L Siegel, Kimberly D Miller, and Ahmedin Jemal. Cancer statis-
34 tics, 2015. *CA: a cancer journal for clinicians*, 65(1):5–29, 2015.
- 35 [3] Roger Stupp, Monika E Hegi, Warren P Mason, Martin J van den Bent,
36 1260 Martin JB Taphoorn, Robert C Janzer, Samuel K Ludwin, Anouk All-
37 geier, Barbara Fisher, Karl Belanger, et al. Effects of radiotherapy with
38 concomitant and adjuvant temozolomide versus radiotherapy alone on sur-
39 vival in glioblastoma in a randomised phase iii study: 5-year analysis of
40 the eortc-ncic trial. *The lancet oncology*, 10(5):459–466, 2009.
- 41 [4] Judith VMG Bovée, Anne-Marie Cleton-Jansen, Antonie HM Taminiau,
42 1265 and Pancras CW Hogendoorn. Emerging pathways in the development
43 of chondrosarcoma of bone and implications for targeted treatment. *The*
44 *lancet oncology*, 6(8):599–607, 2005.
- 45 [5] Marilena Cesari, Franco Bertoni, Patrizia Bacchini, Mario Mercuri,
46 1270 Emanuela Palmerini, and Stefano Ferrari. Mesenchymal chondrosarcoma.
47 an analysis of patients treated at a single institution. *Tumori Journal*, 93
48 (5):423–427, 2007.
- 49 [6] Richard F Riedel, Nicole Larrier, Leslie Dodd, David Kirsch, Salutarior
50 Martinez, and Brian E Brigman. The clinical management of chondrosar-
51 coma. *Current treatment options in oncology*, 10(1-2):94–106, 2009.
- 52 1275 [7] Lars R Holsti. Development of clinical radiotherapy since 1896. *Acta*
53 *Oncologica*, 34(8):995–1003, 1995.
54
55
56
57
58
59
60

- 1
2
3
4
5
6
7
8 [8] Eric J Hall and Amato J Giaccia. *Radiobiology for the Radiologist*. Philadelphia, PA: Lippincott Williams & Wilkins, 2012.
- 9
10
11 1280 [9] Arthur L Boyer and X Yu Cedric. Intensity-modulated radiation therapy
12 with dynamic multileaf collimators. In *Seminars in radiation oncology*,
13 volume 9, pages 48–59. Elsevier, 1999.
- 14
15 [10] Benedick A Fraass. The development of conformal radiation therapy. *Med-*
16 *ical physics*, 22(11):1911–1921, 1995.
- 17
18 1285 [11] Marcel van Herk. Different styles of image-guided radiotherapy. In *Semi-*
19 *nars in radiation oncology*, volume 17, pages 258–267. Elsevier, 2007.
- 20
21 [12] BW Raaymakers, IM Jürgenliemk-Schulz, GH Bol, M Glitzner, ANTJ
22 Kotte, B van Asselen, JCJ de Boer, JJ Bluemink, SL Hackett, MA Moer-
23 1290 land, et al. First patients treated with a 1.5 t mri-linac: clinical proof of
24 concept of a high-precision, high-field mri guided radiotherapy treatment.
25 *Physics in Medicine & Biology*, 62(23):L41, 2017.
- 26
27 [13] Timothy M Zagar, Orit Kaidar-Person, Xiaoli Tang, Ellen E Jones, Jason
28 Matney, Shiva K Das, Rebecca L Green, Arif Sheikh, Amir H Khandani,
29 1295 William H McCartney, et al. Utility of deep inspiration breath hold for
30 left-sided breast radiation therapy in preventing early cardiac perfusion
31 defects: a prospective study. *International Journal of Radiation Oncology**
32 *Biology* Physics*, 97(5):903–909, 2017.
- 33
34 [14] Yuting Lin, Tian Liu, Xiaofeng Yang, Yuenan Wang, and Mohammad K
35 1300 Khan. Respiratory-induced prostate motion using wavelet decomposition
36 of the real-time electromagnetic tracking signal. *International Journal of*
37 *Radiation Oncology* Biology* Physics*, 87(2):370–374, 2013.
- 38
39 [15] Daniela Schulz-Ertner, Oliver Jäkel, and Wolfgang Schlegel. Radiation
40 therapy with charged particles. In *Seminars in radiation oncology*, vol-
41 ume 16, pages 249–259. Elsevier, 2006.
- 42
43 1305 [16] Bahman Emami, J Lyman, A Brown, L Cola, M Goitein, JE Munzenrider,
44 B Shank, LJ Solin, and M Wesson. Tolerance of normal tissue to thera-
45 peutic irradiation. *International Journal of Radiation Oncology* Biology**
46 *Physics*, 21(1):109–122, 1991.
- 47
48 [17] Lawrence B Marks, Ellen D Yorke, Andrew Jackson, Randall K
49 1310 Ten Haken, Louis S Constone, Avraham Eisbruch, Søren M Bentzen, Jiho
50 Nam, and Joseph O Deasy. Use of normal tissue complication probabil-
51 ity models in the clinic. *International Journal of Radiation Oncology**
52 *Biology* Physics*, 76(3):S10–S19, 2010.
- 53
54 [18] JW Hopewell, AD Morris, and A Dixon-Brown. The influence of field size
55 1315 on the late tolerance of the rat spinal cord to single doses of x rays. *The*
56 *British journal of radiology*, 60(719):1099–1108, 1987.
- 57
58 [19] Jean A Laissue, Hans Blattmann, and Daniel N Slatkin. Alban köhler
59 (1874-1947): Inventor of grid therapy, 2012.
- 60

- 1
2
3
4
5
6
7
8 [20] Hualin Zhang, Jian Z Wang, Nina Mayr, Xiang Kong, Jiankui Yuan,
9 1320 Nilendu Gupta, Simon Lo, John Grecula, Joseph Montebello, Douglas
10 Martin, et al. Fractionated grid therapy in treating cervical cancers: Con-
11 ventional fractionation or hypofractionation? *International Journal of*
12 *Radiation Oncology* Biology* Physics*, 70(1):280–288, 2008.
- 13 [21] Silvia Gil, Sukhéna Sarun, Albert Biete, Yolanda Prezado, and Manel
14 1325 Sabés. Survival analysis of f98 glioma rat cells following minibeam or
15 broad-beam synchrotron radiation therapy. *Radiation Oncology*, 6(1):37,
16 2011.
- 17 [22] Yolanda Prezado, Pierre Deman, Pascale Varlet, Gregory Jouvion, Silvia
18 Gil, Céline Le Clec’H, Hélène Bernard, Géraldine Le Duc, and Sukhena
19 1330 Sarun. Tolerance to dose escalation in minibeam radiation therapy applied
20 to normal rat brain: long-term clinical, radiological and histopathological
21 analysis. *Radiation research*, 184(3):314–321, 2015.
- 22 [23] Yolanda Prezado, Sukhena Sarun, Silvia Gil, Pierre Deman, Audrey
23 Bouchet, and Geraldine Le Duc. Increase of lifespan for glioma-bearing
24 1335 rats by using minibeam radiation therapy. *Journal of synchrotron radia-*
25 *tion*, 19(1):60–65, 2012.
- 26 [24] C Peucelle, C Nauraye, A Patriarca, E Hierso, N Fournier-Bidoz,
27 I Martínez-Rovira, and Y Prezado. Proton minibeam radiation therapy:
28 Experimental dosimetry evaluation. *Medical physics*, 42(12):7108–7113,
29 1340 2015.
- 30 [25] Yolanda Prezado, Gregory Jouvion, David Hardy, Annalisa Patriarca,
31 Catherine Nauraye, Judith Bergs, Wilfredo González, Consuelo Guardi-
32 1345 ola, Marjorie Juchaux, Dalila Labiod, et al. Proton minibeam radiation
33 therapy spares normal rat brain: Long-term clinical, radiological and
34 histopathological analysis. *Scientific reports*, 7(1):14403, 2017.
- 35 [26] Elisabeth Schültke, Michael Trippel, Elke Bräuer-Krisch, Michel Renier,
36 Stefan Bartzsch, Herwig Requardt, Máté D Döbrössy, and Guido Nikkhah.
37 Pencilbeam irradiation technique for whole brain radiotherapy: technical
38 1350 and biological challenges in a small animal model. *PLoS One*, 8(1):e54960,
39 2013.
- 40 [27] S. Girst, C. Marx, E. Bräuer-Krisch, A. Bravin, S. Bartzsch, U. Oelfke,
41 C. Greubel, J. Reindl, C. Siebenwirth, O. Zlobinskaya, G. Multhoff,
42 G. Dollinger, T. E. Schmid, and J. J. Wilkens. Improved normal tissue
43 1355 protection by proton and X-ray microchannels compared to homogeneous
44 field irradiation. *Physica Medica*, 31(6):615–620, September 2015. ISSN
45 1120-1797.
- 46 [28] W Zeman, HJ Curtis, and CP Baker. Histopathologic effect of high-
47 energy-particle microbeams on the visual cortex of the mouse brain. *Ra-*
48 *diation research*, 15(4):496–514, 1961.
- 49 [29] Daniel N Slatkin, Per Spanne, FA Dilmanian, and Michael Sandborg.
50 Microbeam radiation therapy. *Medical physics*, 19(6):1395–1400, 1992.
51
52
53
54
55
56
57
58
59
60

- 1
2
3
4
5
6
7
8 [30] D N Slatkin, P Spanne, F A Dilmanian, J-O Gebbers, and J A Laissue.
9 Subacute neuropathological effects of microplanar beams of x-rays from a
10 synchrotron wiggler. *Proc. Natl. Acad. Sci. USA*, 92, 1995.
- 11
12 1365 [31] E. Bräuer-Krisch, R. Serduc, E. A. Siegbahn, G. Le Duc, Y. Prezado,
13 A. Bravin, H. Blattmann, and J. A. Laissue. Effects of pulsed,
14 spatially fractionated, microscopic synchrotron X-ray beams on nor-
15 mal and tumoral brain tissue. *Mutation research*, 704(1-3):160–166,
16 2010. ISSN 0027-5107. doi: 10.1016/j.mrrev.2009.12.003. URL
17 <http://www.ncbi.nlm.nih.gov/pubmed/20034592>.
- 18 [32] H Blattmann, J-O Gebbers, E Bräuer-Krisch, A Bravin, G Le Duc,
19 W Burkard, M Di Michiel, V Djonov, DN Slatkin, J Stepanek, et al.
20 Applications of synchrotron x-rays to radiotherapy. *Nuclear Instruments*
21 *and Methods in Physics Research Section A: Accelerators, Spectrometers,*
22 1375 *Detectors and Associated Equipment*, 548(1-2):17–22, 2005.
- 23 [33] Jean A Laissue, Stefan Bartzsch, Hans Blattmann, Elke Bräuer-Krisch,
24 Alberto Bravin, Dominique Dalléry, Valentin Djonov, Albert L Hanson,
25 John W Hopewell, Barbara Kaser-Hotz, et al. Response of the rat spinal
26 cord to x-ray microbeams. *Radiotherapy and oncology*, 106(1):106–111,
27 2013.
28 1380
- 29 [34] Naritoshi Mukumoto, Masao Nakayama, Hiroaki Akasaka, Yasuyuki
30 Shimizu, Saki Osuga, Daisuke Miyawaki, Kenji Yoshida, Yasuo Ejima,
31 Yasushi Miura, Keiji Umetani, et al. Sparing of tissue by using micro-slit-
32 beam radiation therapy reduces neurotoxicity compared with broad-beam
33 radiation therapy. *Journal of radiation research*, 58(1):17–23, 2017.
34 1385
- 35 [35] Lloyd ML Smyth, Jacqueline F Donoghue, Jessica A Ventura, Jayde Liv-
36 ingtonstone, Tracy Bailey, Liam RJ Day, Jeffrey C Crosbie, and Peter AW
37 Rogers. Comparative toxicity of synchrotron and conventional radiation
38 therapy based on total and partial body irradiation in a murine model.
39 *Scientific reports*, 8(1):12044, 2018.
40 1390
- 41 [36] Raphaël Serduc, Audrey Bouchet, Elke Bräuer-Krisch, Jean A. Lais-
42 sue, Jenny Spiga, Sukhéna Sarun, Alberto Bravin, Caroline Fonta, Luc
43 Renaud, Jean Boutonnat, Erik Albert Siegbahn, François Estève, and
44 Géraldine Le Duc. Synchrotron microbeam radiation therapy for rat brain
45 tumor palliation—influence of the microbeam width at constant valley
46 dose. *Physics in Medicine and Biology*, 54(21):6711, November 2009. ISSN
47 0031-9155. doi: 10.1088/0031-9155/54/21/017.
48 1395
- 49 [37] E Schültke, E Bräuer-Krisch, H Blattmann, H Requardt, JA Laissue, and
50 G Hildebrandt. Survival of rats bearing advanced intracerebral f 98 tumors
51 after glutathione depletion and microbeam radiation therapy: conclusions
52 from a pilot project. *Radiation Oncology*, 13(1):89, 2018.
53 1400
- 54 [38] Mohammad Johari Ibahim, Jeffrey C Crosbie, Yuqing Yang, Marina Za-
55 itseva, Andrew W Stevenson, Peter AW Rogers, and Premila Paiva. An
56 evaluation of dose equivalence between synchrotron microbeam radiation
57 therapy and conventional broadbeam radiation using clonogenic and cell
58 impedance assays. *PLoS One*, 9(6):e100547, 2014.
59 1405
60

- 1
2
3
4
5
6
7
8 [39] Elisabeth Schültke, Bernhard HJ Juurlink, Khalid Ataelmannan, Jean
9 Laissue, Hans Blattmann, Elke Bräuer-Krisch, Alberto Bravin, Joanna
10 Minczewska, Jeffrey Crosbie, Hadi Taherian, et al. Memory and survival
11 1410 after microbeam radiation therapy. *European journal of radiology*, 68(3):
12 S142–S146, 2008.
- 13
14 [40] Raphaël Serduc, Yohan van de Looij, Gilles Francony, Olivier Ver-
15 donck, Boudewijn van der Sanden, Jean Laissue, Régine Farion, Elke
16 Bräuer-Krisch, Erik Albert Siegbahn, Alberto Bravin, Yolanda Prezado,
17 1415 Christoph Segebarth, Chantal Rémy, and Hana Lahrech. Characteriza-
18 tion and quantification of cerebral edema induced by synchrotron x-ray
19 microbeam radiation therapy. *Physics in Medicine and Biology*, 53(5):
20 1153, March 2008. ISSN 0031-9155. doi: 10.1088/0031-9155/53/5/001.
- 21
22 [41] JA Laissue, H Blattmann, HP Wagner, MA Grotzer, and DN Slatkin.
23 1420 Prospects for microbeam radiation therapy of brain tumours in children to
24 reduce neurological sequelae. *Developmental Medicine & Child Neurology*,
25 49(8):577–581, 2007.
- 26
27 [42] Boudewijn Van Der Sanden, Elke Bräuer-Krisch, Erik Albert Siegbahn,
28 Clément Ricard, Jean-Claude Vial, and Jean Laissue. Tolerance of arteries
29 1425 to microplanar x-ray beams. *International Journal of Radiation Oncology**
30 *Biology* Physics*, 77(5):1545–1552, 2010.
- 31
32 [43] M Miura, H Blattmann, E Brauer-Krisch, A Bravin, AL Hanson,
33 MM Nawrocky, PL Micca, DN Slatkin, and JA Laissue. Radiosurgi-
34 1430 cal palliation of aggressive murine scvii squamous cell carcinomas using
35 synchrotron-generated x-ray microbeams. *The British journal of radiol-*
36 *ogy*, 79(937):71–75, 2006.
- 37
38 [44] Jean A Laissue, Gabrielle Geiser, Per O Spanne, F Avraham Dilm-
39 1435 nian, Jan-Olaf Gebbers, Marianne Geiser, Xiao-Ye Wu, Michael S Makar,
40 Peggy L Micca, Marta M Nawrocky, et al. Neuropathology of ablation of
41 rat gliosarcomas and contiguous brain tissues using a microplanar beam
42 of synchrotron-wiggler-generated x rays. *International journal of cancer*,
43 78(5):654–660, 1998.
- 44
45 [45] Audrey Bouchet, Elke Bräuer-Krisch, Yolanda Prezado, Michèle El At-
46 1440 ifi, Léonid Rogalev, Céline Le Clec’h, Jean Albert Laissue, Laurent Pel-
47 letier, and Géraldine Le Duc. Better efficacy of synchrotron spatially
48 microfractionated radiation therapy than uniform radiation therapy on
49 glioma. *International Journal of Radiation Oncology* Biology* Physics*,
50 95(5):1485–1494, 2016.
- 51
52 [46] Stefan Bartzsch, Craig Cummings, Stephan Eismann, and Uwe Oelfke.
53 1445 A preclinical microbeam facility with a conventional x-ray tube. *Medical*
54 *physics*, 43(12):6301–6308, 2016.
- 55
56 [47] Mike Hadsell, Guohua Cao, Jian Zhang, Laurel Burk, Torsten Schreiber,
57 1450 Eric Schreiber, Sha Chang, Jianping Lu, and Otto Zhou. Pilot study
58 for compact microbeam radiation therapy using a carbon nanotube field
59 emission micro-ct scanner. *Medical physics*, 41(6Part1), 2014.
- 60

- 1
2
3
4
5
6
7
8 [48] Jeffrey C Crosbie, Robin L Anderson, Kai Rothkamm, Christina M Restall, Leonie Cann, Saleela Ruwanpura, Sarah Meachem, Naoto Yagi, Imants Svalbe, Robert A Lewis, et al. Tumor cell response to synchrotron microbeam radiation therapy differs markedly from cells in normal tissues. *International Journal of Radiation Oncology* Biology* Physics*, 77 (3):886–894, 2010.
9
10
11
12 1455
13
14
15 [49] Audrey Bouchet, Nathalie Sakakini, Michèle El Atifi, Céline Le Clec'h, Elke Bräuer-Krisch, Léonid Rogalev, Jean Albert Laissue, Pascal Rihet, Géraldine Le Duc, and Laurent Pelletier. Identification of areg and plk1 pathway modulation as a potential key of the response of intracranial 9l tumor to microbeam radiation therapy. *International journal of cancer*, 136(11):2705–2716, 2015.
16
17 1460
18
19
20
21 [50] Audrey Bouchet, Nathalie Sakakini, Michèle El Atifi, Céline Le Clec'h, Elke Brauer, Anaïck Moisan, Pierre Deman, Pascal Rihet, Géraldine Le Duc, and Laurent Pelletier. Early gene expression analysis in 9l orthotopic tumor-bearing rats identifies immune modulation in molecular response to synchrotron microbeam radiation therapy. *PLoS One*, 8(12):e81874, 2013.
22
23 1465
24
25
26
27 [51] MJ Ibahim, Y Yang, JC Crosbie, A Stevenson, L Cann, P Paiva, and PA Rogers. Eosinophil-associated gene pathways but not eosinophil numbers are differentially regulated between synchrotron microbeam radiation treatment and synchrotron broad-beam treatment by 48 hours postirradiation. *Radiation research*, 185(1):60–68, 2015.
28
29 1470
30
31
32
33 [52] Yuqing Yang, Jeffrey C Crosbie, Premila Paiva, Mohammad Ibahim, Andrew Stevenson, and Peter AW Rogers. In vitro study of genes and molecular pathways differentially regulated by synchrotron microbeam radiotherapy. *Radiation research*, 182(6):626–639, 2014.
34
35 1475
36
37
38 [53] Carl N Sprung, Yuqing Yang, Helen B Forrester, Jason Li, Marina Zaitseva, Leonie Cann, Tina Restall, Robin L Anderson, Jeffrey C Crosbie, and Peter AW Rogers. Genome-wide transcription responses to synchrotron microbeam radiotherapy. *Radiation research*, 178(4):249–259, 2012.
39
40 1480
41
42 [54] Audrey Bouchet, Benjamin Lemasson, Thomas Christen, Marine Potez, Claire Rome, Nicolas Coquery, Céline Le Clec'h, Anaïck Moisan, Elke Bräuer-Krisch, Géraldine Leduc, et al. Synchrotron microbeam radiation therapy induces hypoxia in intracerebral gliosarcoma but not in the normal brain. *Radiotherapy and oncology*, 108(1):143–148, 2013.
43
44 1485
45
46
47 [55] Audrey Bouchet, Benjamin Lemasson, Géraldine Le Duc, Cécile Maisin, Elke Bräuer-Krisch, Erik Albert Siegbahn, Luc Renaud, Enam Khalil, Chantal Rémy, Cathy Poillot, et al. Preferential effect of synchrotron microbeam radiation therapy on intracerebral 9l gliosarcoma vascular networks. *International Journal of Radiation Oncology* Biology* Physics*, 78 (5):1503–1512, 2010.
48
49 1490
50
51
52
53 [56] Jayde Livingstone, Jean-François Adam, Jeffrey C Crosbie, Chris J Hall, Jessica E Lye, Jonathan McKinlay, Daniele Pelliccia, Frédéric Pouzoulet, Yolanda Prezado, Andrew W Stevenson, et al. Preclinical radiotherapy
54
55 1495
56
57
58
59
60

- at the australian synchrotron’s imaging and medical beamline: instrumentation, dosimetry and a small-animal feasibility study. *Journal of Synchrotron Radiation*, 24(4), 2017.
- [57] M Renier, Th Brochard, C Nemoz, H Requardt, E Bräuer, F Esteve, J Balosso, P Suortti, J Baruchel, H Elleaume, et al. The radiotherapy clinical trials projects at the esrf: technical aspects. *European journal of radiology*, 68(3):S147–S150, 2008.
- [58] Vincent Favaudon, Laura Caplier, Virginie Monceau, Frédéric Pouzoulet, Mano Sayarath, Charles Fouillade, Marie-France Poupon, Isabel Brito, Philippe Hupé, Jean Bourhis, et al. Ultrahigh dose-rate flash irradiation increases the differential response between normal and tumor tissue in mice. *Science translational medicine*, 6(245):245ra93–245ra93, 2014.
- [59] Pierre Montay-Gruel, Kristoffer Petersson, Maud Jaccard, Gaël Boivin, Jean-François Germond, Benoit Petit, Raphaël Doenlen, Vincent Favaudon, François Bochud, Claude Bailat, et al. Irradiation in a flash: unique sparing of memory in mice after whole brain irradiation with dose rates above 100 gy/s. *Radiotherapy and Oncology*, 124(3):365–369, 2017.
- [60] Pierre Montay-Gruel, Audrey Bouchet, Maud Jaccard, David Patin, Raphael Serduc, Warren Aim, Kristoffer Petersson, Benoit Petit, Claude Bailat, Jean Bourhis, et al. X-rays can trigger the flash effect: Ultrahigh dose-rate synchrotron light source prevents normal brain injury after whole brain irradiation in mice. *Radiotherapy and Oncology*, 129(3):582–588, 2018.
- [61] Marie-Catherine Vozenin, Pauline De Fornel, Kristoffer Petersson, Vincent Favaudon, Maud Jaccard, Jean-François Germond, Benoit Petit, Marco Burki, Gisèle Ferrand, David Patin, et al. The advantage of flash radiotherapy confirmed in mini-pig and cat-cancer patients. *Clinical Cancer Research*, 25(1):35–42, 2019.
- [62] Elisabeth Schültke, Jacques Balosso, Thomas Breslin, Guido Cavaletti, Valentin Djonov, Francois Esteve, Michael Grotzer, Guido Hildebrandt, Alexander Valdman, and Jean Laissue. Microbeam radiation therapy—grid therapy and beyond: a clinical perspective. *The British journal of radiology*, 90(1078):20170073, 2017.
- [63] Audrey Bouchet, Marine Potez, Nicolas Coquery, Claire Rome, Benjamin Lemasson, Elke Bräuer-Krisch, Chantal Rémy, Jean Laissue, Emmanuel L Barbier, Valentin Djonov, et al. Permeability of brain tumor vessels induced by uniform or spatially microfractionated synchrotron radiation therapies. *International Journal of Radiation Oncology* Biology* Physics*, 98(5):1174–1182, 2017.
- [64] Daniel Brönnimann, Audrey Bouchet, Christoph Schneider, Marine Potez, Raphaël Serduc, Elke Bräuer-Krisch, Werner Graber, Stephan Von Gunten, Jean Albert Laissue, and Valentin Djonov. Synchrotron microbeam irradiation induces neutrophil infiltration, thrombocyte attachment and selective vascular damage in vivo. *Scientific reports*, 6:33601, 2016.

- 1
2
3
4
5
6
7
8 [65] Audrey Bouchet, Ahcene Boumendjel, Enam Khalil, Raphael Serduc, Elke
9 Bräuer, Erik Albert Siegbahn, Jean A Laissue, and Jean Boutonnat. Chal-
10 cone jai-51 improves efficacy of synchrotron microbeam radiation therapy
11 of brain tumors. *Journal of synchrotron radiation*, 19(4):478–482, 2012.
- 12
13 [66] Pierrick Régnard, Elke Bräuer-Krisch, Irène Tropès, Jani Keyriläinen,
14 1545 Alberto Bravin, and Géraldine Le Duc. Enhancement of survival of 9l
15 gliosarcoma bearing rats following intracerebral delivery of drugs in com-
16 bination with microbeam radiation therapy. *European journal of radiology*,
17 68(3):S151–S155, 2008.
- 18 [67] HM Smilowitz, H Blattmann, E Bräuer-Krisch, A Bravin, M Di Michiel,
19 1550 J-O Gebbers, AL Hanson, N Lyubimova, DN Slatkin, J Stepanek, et al.
20 Synergy of gene-mediated immunoprophylaxis and microbeam radiation
21 therapy for advanced intracerebral rat 9l gliosarcomas. *Journal of neuro-*
22 *oncology*, 78(2):135–143, 2006.
- 23 [68] Pantaleo Romanelli and Alberto Bravin. Synchrotron-generated mi-
24 1555 crobeam radiosurgery: a novel experimental approach to modulate brain
25 function. *Neurological research*, 33(8):825–831, 2011.
- 26 [69] Raphaël Serduc, Elke Bräuer-Krisch, Erik A. Siegbahn, Audrey Bouchet,
27 Benoit Pouyatos, Romain Carron, Nicolas Pannetier, Luc Renaud, Gilles
28 Berruyer, Christian Nemoz, Thierry Brochard, Chantal Rémy, Em-
29 manuel L. Barbier, Alberto Bravin, Géraldine Le Duc, Antoine Depaulis,
30 1560 François Estève, and Jean A. Laissue. High-precision radiosurgical dose
31 delivery by interlaced microbeam arrays of high-flux low-energy syn-
32 chrotron x-rays. *PLOS ONE*, 5(2):1–12, 02 2010. doi: 10.1371/jour-
33 nal.pone.0009028.
- 34 [70] F Avraham Dilmanian, Arthur L Jenkins III, John A Olschowka, Zhong
35 1565 Zhong, Jane Y Park, Nicole R Desnoyers, Stanislaw Sobotka, Giovanna R
36 Fois, Catherine R Messina, Marjorie Morales, et al. X-ray microbeam
37 irradiation of the contusion-injured rat spinal cord temporarily improves
38 hind-limb function. *Radiation research*, 179(1):76–88, 2012.
- 39 [71] Benoît Pouyatos, Raphaël Serduc, Mathilde Chipaux, Tanguy Chabrol,
40 1570 Elke Bräuer-Krisch, Christian Nemoz, Hervé Mathieu, Olivier David, Luc
41 Renaud, Yolanda Prezado, et al. Synchrotron x-ray interlaced microbeams
42 suppress paroxysmal oscillations in neuronal networks initiating general-
43 ized epilepsy. *Neurobiology of disease*, 51:152–160, 2013.
- 44 [72] Erminia Fardone, Benoît Pouyatos, Elke Bräuer-Krisch, Stefan Bartzsch,
45 1575 Hervé Mathieu, Herwig Requardt, Domenico Bucci, Giacomo Barbone,
46 Paola Coan, Giuseppe Battaglia, et al. Synchrotron-generated mi-
47 crobeams induce hippocampal transections in rats. *Scientific reports*, 8
48 (1):184, 2018.
- 49 [73] FR Elder, AM Gurewitsch, RV Langmuir, and HC Pollock. Radiation
50 1580 from electrons in a synchrotron. *Physical Review*, 71(11):829, 1947.
- 51 [74] Kwang-Je Kim. Brightness, coherence and propagation characteristics
52 of synchrotron radiation. *Nuclear Instruments and Methods in Physics*

- 1
2
3
4
5
6
7
8
9
10
11
12
13
14
15
16
17
18
19
20
21
22
23
24
25
26
27
28
29
30
31
32
33
34
35
36
37
38
39
40
41
42
43
44
45
46
47
48
49
50
51
52
53
54
55
56
57
58
59
60
- 1585 *Research Section A: Accelerators, Spectrometers, Detectors and Associated Equipment*, 246(1-3):71–76, 1986.
- [75] Philip Duke. *Synchrotron radiation: production and properties*, volume 3. Oxford University Press, 2009.
- [76] Herman Winick and Sebastian Doniach. *Synchrotron radiation research*. Springer Science & Business Media, 2012.
- 1590 [77] Jeffrey C Crosbie, Pauline Fournier, Stefan Bartzsch, Mattia Donzelli, Iwan Cornelius, Andrew W Stevenson, Herwig Requardt, and Elke Braeuer-Krisch. Energy spectra considerations for synchrotron radiotherapy trials on the id17 bio-medical beamline at the european synchrotron radiation facility. *Journal of synchrotron radiation*, 22(4):1035–1041, 2015.
- 1595 [78] Jenny Spiga, EA Siegbahn, E Brauer-Krisch, P Randaccio, and A Bravin. Geant4 simulations for microbeam radiation therapy (mrt) dosimetry. In *Nuclear Science Symposium Conference Record, 2007. NSS'07. IEEE*, volume 4, pages 2571–2575. IEEE, 2007.
- 1600 [79] Mattia Donzelli, Elke Bräuer-Krisch, Uwe Oelfke, Jan J Wilkens, and Stefan Bartzsch. Hybrid dose calculation: a dose calculation algorithm for microbeam radiation therapy. *Physics in Medicine & Biology*, 63(4):045013, 2018.
- 1605 [80] I. Martínez-Rovira, J. Sempau, and Y. Prezado. Development and commissioning of a monte carlo photon beam model for the forthcoming clinical trials in microbeam radiation therapy. *Medical Physics*, 39(1):119–131, January 2012. ISSN 0094-2405. doi: 10.1118/1.3665768.
- 1610 [81] Iwan Cornelius, Susanna Guatelli, Pauline Fournier, Jeffrey C Crosbie, Manuel Sanchez del Rio, Elke Bräuer-Krisch, Anatoly Rosenfeld, and Michael Lerch. Benchmarking and validation of a geant4-shadow monte carlo simulation for dose calculations in microbeam radiation therapy. *Journal of synchrotron radiation*, 21(3):518–528, 2014.
- 1615 [82] Andrew W Stevenson, Jeffrey C Crosbie, Christopher J Hall, Daniel Häusermann, Jayde Livingstone, and Jessica E Lye. Quantitative characterization of the x-ray beam at the australian synchrotron imaging and medical beamline (imbl). *Journal of synchrotron radiation*, 24(1):110–141, 2017.
- 1620 [83] Tomasz W Wysokinski, Dean Chapman, Gregg Adams, Michel Renier, Pekka Suortti, and William Thomlinson. Beamlines of the biomedical imaging and therapy facility at the canadian light source—part 3. *Nuclear Instruments and Methods in Physics Research Section A: Accelerators, Spectrometers, Detectors and Associated Equipment*, 775:1–4, 2015.
- 1625 [84] M Renier, T Brochard, C Nemoz, and W Thomlinson. A white-beam fast-shutter for microbeam radiation therapy at the esrf. *Nuclear Instruments and Methods in Physics Research Section A: Accelerators, Spectrometers, Detectors and Associated Equipment*, 479(2-3):656–660, 2002.

- 1
2
3
4
5
6
7
8 [85] David W Archer. Collimator for producing an array of microbeams,
9 June 23 1998. US Patent 5,771,270.
- 10
11 [86] E Bräuer-Krisch, A Bravin, L Zhang, E Siegbahn, J Stepanek,
12 H Blattmann, DN Slatkin, J-O Gebbers, M Jasmin, and JA Laissue.
1630 Characterization of a tungsten/gas multislit collimator for microbeam ra-
13 diation therapy at the european synchrotron radiation facility. *Review of*
14 *scientific instruments*, 76(6):064303, 2005.
- 15
16 [87] E Bräuer-Krisch, H Requardt, T Brochard, G Berruyer, M Renier,
17 JA Laissue, and A Bravin. New technology enables high precision mul-
18 1635 tislit collimators for microbeam radiation therapy. *Review of scientific*
19 *instruments*, 80(7):074301, 2009.
- 20
21 [88] E Bräuer-Krisch, C Nemoz, Th Brochard, G Berruyer, M Renier, B Pouy-
22 atos, and R Serduc. The preclinical set-up at the id17 biomedical beam-
23 line to achieve high local dose deposition using interlaced microbeams.
24 1640 In *Journal of Physics: Conference Series*, volume 425, page 022001. IOP
25 Publishing, 2013.
- 26
27 [89] T W Wysokinski, D Chapman, G Adams, M Renier, P Suortti,
28 and W Thomlinson. Beamlines of the biomedical imaging and
29 therapy facility at the canadian light source - part 2. *Jour-*
30 1645 *nal of Physics: Conference Series*, 425(7):072013, 2013. URL
31 <http://stacks.iop.org/1742-6596/425/i=7/a=072013>.
- 32
33 [90] Raphaël Serduc, Gilles Berruyer, Thierry Brochard, Michel Renier, and
34 Christian Nemoz. In vivo pink-beam imaging and fast alignment proce-
35 1650 dure for rat brain lesion microbeam radiation therapy. *Journal of syn-*
36 *chrotron radiation*, 17(3):325–331, 2010.
- 37
38 [91] Pantaleo Romanelli, Erminia Fardone, Giuseppe Battaglia, Elke Bräuer-
39 Krisch, Yolanda Prezado, Herwig Requardt, Geraldine Le Duc, Christian
40 Nemoz, David J Ansel, Jenny Spiga, et al. Synchrotron-generated mi-
41 1655 crobeam sensorimotor cortex transections induce seizure control without
42 disruption of neurological functions. *PloS one*, 8(1):e53549, 2013.
- 43
44 [92] Lei Zhang, Hong Yuan, Laurel M Burk, Christy R Inscoe, Michael J Had-
45 sell, Pavel Chtcheprov, Yueh Z Lee, Jianping Lu, Sha Chang, and Otto
46 1660 Zhou. Image-guided microbeam irradiation to brain tumour bearing mice
47 using a carbon nanotube x-ray source array. *Physics in medicine and*
48 *biology*, 59(5):1283, 2014.
- 49
50 [93] M Hadsell, J Zhang, P Laganis, F Sprenger, J Shan, L Zhang, L Burk,
51 H Yuan, S Chang, J Lu, et al. A first generation compact microbeam
52 radiation therapy system based on carbon nanotube x-ray technology.
53 *Applied physics letters*, 103(18):183505, 2013.
- 54
55 [94] Christian Nemoz, Astrid Kibleur, Jean-Noël Hyacinthe, Gilles Berruyer,
56 1665 Thierry Brochard, E Brauer-Krisch, Géraldine Le Duc, Emmanuel Brun,
57 Hélène Elleaume, and Raphaël Serduc. In vivo pink-beam imaging and
58 fast alignment procedure for rat brain tumor radiation therapy. *Journal*
59 *of synchrotron radiation*, 23(1):339–343, 2016.
- 60

- 1
2
3
4
5
6
7
8 1670 [95] Daniele Pelliccia, Christopher M Poole, Jayde Livingstone, Andrew W
9 Stevenson, Lloyd ML Smyth, Peter AW Rogers, Daniel Häusermann, and
10 Jeffrey C Crosbie. Image guidance protocol for synchrotron microbeam
11 radiation therapy. *Journal of synchrotron radiation*, 23(2):566–573, 2016.
- 12
13 [96] Daniele Pelliccia, Jeffrey C Crosbie, and Kieran G Larkin. Phase con-
14 1675 trast image guidance for synchrotron microbeam radiotherapy. *Physics in
15 medicine and biology*, 61(16):5942, 2016.
- 16 [97] Mattia Donzelli, Elke Bräuer-Krisch, Christian Nemoz, Thierry Brochard,
17 and Uwe Oelfke. Conformal image-guided microbeam radiation therapy
18 at the esrf biomedical beamline id17. *Medical physics*, 43(6):3157–3167,
19 1680 2016.
- 20 [98] Mattia Donzelli. *Improving dose calculation and treatment planning tech-
21 niques for microbeam radiation therapy with computational methods*. PhD
22 thesis, University of London, 2018.
- 23
24 [99] Francisco Machado de Sola, Manuel Vilches, Yolanda Prezado, and An-
25 1685 tonio M Lallena. Impact of cardiosynchronous brain pulsations on monte
26 carlo calculated doses for synchrotron micro-and minibeam radiation ther-
27 apy. *Medical physics*, 45(7):3379–3390, 2018.
- 28
29 [100] Mattia Donzelli, Uwe Oelfke, and Elke Brauer-Krisch. Introducing the
30 concept of spiral microbeam radiation therapy (spiralmrt). *Physics in
31 1690 medicine and biology*, 2019.
- 32
33 [101] Marek J Maryanski, John C Gore, Richard P Kennan, and Robert J
34 Schulz. Nmr relaxation enhancement in gels polymerized and cross-linked
35 by ionizing radiation: a new approach to 3d dosimetry by mri. *Magnetic
36 resonance imaging*, 11(2):253–258, 1993.
- 37
38 1695 [102] Yves De Deene, C Hurley, A Venning, K Vergote, Melissa Mather,
39 BJ Healy, and C Baldock. A basic study of some normoxic polymer gel
40 dosimeters. *Physics in Medicine & Biology*, 47(19):3441, 2002.
- 41
42 [103] Christian Bayreder, Dietmar Georg, Ewald Moser, and Andreas Berg.
43 Basic investigations on the performance of a normoxic polymer gel with
44 1700 tetrakis-hydroxy-methyl-phosphonium chloride as an oxygen scavenger:
45 Reproducibility, accuracy, stability, and dose rate dependence. *Medical
46 physics*, 33(7Part1):2506–2518, 2006.
- 47
48 [104] Simon J Doran, Thierry Brochard, John Adamovics, Nikola Krstajic, and
49 1705 Elke Bräuer-Krisch. An investigation of the potential of optical computed
50 tomography for imaging of synchrotron-generated x-rays at high spatial
51 resolution. *Physics in Medicine & Biology*, 55(5):1531, 2010.
- 52
53 [105] C-M Ma, CW Coffey, LA DeWerd, C Liu, R Nath, SM Seltzer, and JP Se-
54 untjens. Aapm protocol for 40–300 kv x-ray beam dosimetry in radiother-
55 apy and radiobiology. *Medical physics*, 28(6):868–893, 2001.
- 56
57 1710 [106] EA Siegbahn, E Bräuer-Krisch, J Stepanek, H Blattmann, JA Laissue, and
58 A Bravin. Dosimetric studies of microbeam radiation therapy (mrt) with
59 monte carlo simulations. *Nuclear Instruments and Methods in Physics
60*

- 1
2
3
4
5
6
7
8 *Research Section A: Accelerators, Spectrometers, Detectors and Associated*
9 *Equipment*, 548(1-2):54–58, 2005.
- 10
11 1715 [107] Pauline Fournier, Iwan Cornelius, Mattia Donzelli, Herwig Requardt,
12 Christian Nemoz, Marco Petasecca, Elke Bräuer-Krisch, Anatoly Rosen-
13 feld, and Michael Lerch. X-tream quality assurance in synchrotron x-ray
14 microbeam radiation therapy. *Journal of synchrotron radiation*, 23(5):
15 1180–1190, 2016.
- 16
17 1720 [108] P Andreo, D T Burns, K Hohlfeld, M S Huq, T Kanai, F Laitano, V G
18 Smythe, and S Vynckier. Absorbed dose determination in external beam
19 radiotherapy. Technical Reports Series No. 398, International Atomic En-
20 ergy Agency, Vienna, Austria, 2000.
- 21
22 [109] Charles P Poole. *Electron spin resonance: a comprehensive treatise on*
23 *experimental techniques*. Courier Corporation, 1996.
- 24
25 [110] Arthur Schweiger and Gunnar Jeschke. *Principles of pulse electron para-*
26 *magnetic resonance*. Oxford University Press on Demand, 2001.
- 27
28 [111] Mathias Anton. Development of a secondary standard for the absorbed
29 dose to water based on the alanine epr dosimetry system. *Applied radiation*
30 *and isotopes*, 62(5):779–795, 2005.
- 31
32 [112] Matias Anton and Steven Lelie. *Alanine dosimetry: uncertainty com-*
33 *ponents*. Physikalisch-Technische Bundesanstalt Braunschweig und Berlin,
34 2009.
- 35
36 1735 [113] S. Yasser S. Soliman Soliman, Paolo Pellicoli, W.B. Beshira, Atef A.
37 Abdel-Fattaha, Ramy Amer Fahima, Michael Krisch, and Elke Bräuer-
38 Krisch. A comparative dosimetry of alanine dosimeters with a ptw pin-
39 point chamber at ultra-high dose rates of synchrotron radiation. *submitted*
40 *to Physica Medica*, 2019.
- 41
42 [114] JC Crosbie, I Svalbe, SM Midgley, N Yagi, PA Walton Rogers, and
43 RA Lewis. A method of dosimetry for synchrotron microbeam radia-
44 tion therapy using radiochromic films of different sensitivity. *Physics in*
45 *Medicine & Biology*, 53(23):6861, 2008.
- 46
47 1745 [115] Elke Bräuer-Krisch, Jean-Francois Adam, Enver Alagoz, Stefan Bartzsch,
48 Jeff Crosbie, Carlos DeWagter, Andrew Dipuglia, Mattia Donzelli, Simon
49 Doran, Pauline Fournier, et al. Medical physics aspects of the synchrotron
50 radiation therapies: Microbeam radiation therapy (mrt) and synchrotron
51 stereotactic radiotherapy (ssrt). *Physica Medica*, 31(6):568–583, 2015.
- 52
53 [116] Nobuteru Nariyama, Takuji Ohigashi, Keiji Umetani, Kunio Shinohara,
54 Hiroki Tanaka, Akira Maruhashi, Genro Kashino, Ai Kurihara, Takeshi
55 Kondob, Manabu Fukumoto, and Koji Ono. Spectromicroscopic film
56 dosimetry for high-energy microbeam from synchrotron radiation. *Ap-*
57 *plied Radiation and Isotopes*, 67:155–159, 2009.
- 58
59 [117] Stefan Bartzsch, Johanna Lott, Katrin Welsch, Elke Bräuer-Krisch, and
60 Uwe Oelfke. Micrometer-resolved film dosimetry using a microscope in
61 microbeam radiation therapy. *Medical physics*, 42(7):4069–4079, 2015.

- 1
2
3
4
5
6
7
8 [118] Paolo Pelliccioli, Stefan Bartzsch, Mattia Donzelli, Krisch Michael, and
9 Elke Bräuer-Krisch. High resolution radiochromic film dosimetry: compar-
10 ison of a microdensitometer and an optical microscope. *submitted to*
11 *Physica Medica*, 2019.
- 12
13 1760 [119] Lerch ML. Kron T. Bräuer-Krisch E. Bravin A. Holmes-Siedle A. Rosen-
14 feld, AB. and BJ. Allen. Feasibility study of online high-spatial-resolution
15 mosfet dosimetry in static and pulsed x-ray radiation fields. *IEEE Trans-*
16 *actions on Nuclear Science*, 48(6):2061–2068, 2001.
- 17
18 [120] El Bräuer-Krisch, A Bravin, M Lerch, A Rosenfeld, J Stepanek,
19 M Di Michiel, and JA Laissue. Mosfet dosimetry for microbeam radiation
20 therapy at the european synchrotron radiation facility. *Medical physics*,
21 30(4):583–589, 2003.
- 22
23 [121] EA Siegbahn, E Bräuer-Krisch, Alberto Bravin, Heidi Nettelbeck, MLF
24 Lerch, and Anatoly B Rosenfeld. Mosfet dosimetry with high spatial
25 resolution in intense synchrotron-generated x-ray microbeams. *Medical*
26 *physics*, 36(4):1128–1137, 2009.
- 27
28 [122] Duggan L. Smith T. Rosenfeld-A. Butson M. Kaplan G.-Howlett S. Hy-
29 odo K. Kron, T. Dose response of various radiation detectors to syn-
30 chrotron radiation. *Physics in medicine and biology*, 43(11):3235–3259,
31 1998.
- 32
33 [123] M De Felici, R Felici, M Sanchez del Rio, C Ferrero, T Bacarian, and
34 FA Dilmanian. Dose distribution from x-ray microbeam arrays applied
35 to radiation therapy: An egs4 monte carlo study. *Medical physics*, 32(8):
36 2455–2463, 2005.
- 37
38 [124] Butson M.J. Cheung, T. and P.K.N. Yu. Energy dependence corrections
39 to mosfet dosimetric sensitivity. *Australasian Physical & Engineering Sci-*
40 *ences in Medicine*, 32(1):16–17, 2009.
- 41
42 [125] H. Requardt A. Cullen E. Baloglow E. Bräuer-Krisch A. Bravin M. Rein-
43 hard R. Siegele V. Perevertaylo M. Lerch, H. Nettelbeck and A. Rosenfeld.
44 Multichannel silicon detectors for on-line synchrotron x-ray microbeam
45 radiation dosimetry. In *10th International Conference on Synchrotron*
46 *Radiation Instrumentation, Melbourne, September 2009.*
- 47
48 [126] Petasecca M. Cullen A. Hamad A. Requardt H. Bräuer-Krisch-E. Bravin
49 A. Perevertaylo V. Lerch, M. and A. B. Rosenfeld. Dosimetry of in-
50 tensive synchrotron microbeams. *Radiation Measurements*, 46(12):1560–
51 1565, 2011.
- 52
53 [127] Cullen A. Fuduli I. Espinoza A. Porumb C. Stanton-C.-Aldosari A.
54 Bräuer-Krisch E. Requardt H. Bravin A. Rosenfeld A.B. Petasecca, M.
55 and M.L.F. Lerch. Dosimetry of intensive synchrotron microbeams. *Ra-*
56 *diation Measurements*, 46(12):1560–1565, 2011.
- 57
58 [128] Pauline Fournier, Iwan Cornelius, Andrew Dipuglia, Matthew Cameron,
59 Jeremy A Davis, Ashley Cullen, Marco Petasecca, Anatoly B Rosenfeld,
60 Elke Bräuer-Krisch, Daniel Häusermann, et al. X-tream dosimetry of

- highly brilliant x-ray microbeams in the mrt hutch of the australian synchrotron. *Radiation Measurements*, 106:405–411, 2017.
- [129] Paino J.R. Dipuglia A. Cameron M. Siegele R. Pastuovic-Z.-Petasecca M. Perevertaylo-V.L. Rosenfeld A.B. Lerch M.L.F. Davis, J.A. Characterisation and evaluation of a pnp strip detector for synchrotron microbeam radiation therapy. *Biomedical Physics and Engineering Express*, 4(4):044002, 2018.
- [130] E. Klosowski M. Czopyka L. Olkoa P. Ptaszkiewiczza, M. Bräuer-Krisch. Tld dosimetry for microbeam radiation therapy at the european synchrotron radiation facility. *Radiation Measurements*, 43(2-6):990–993, 2008.
- [131] GM Akselrod, MS Akselrod, ER Benton, and N Yasuda. A novel al₂o₃ fluorescent nuclear track detector for heavy charged particles and neutrons. *Nuclear Instruments and methods in physics Research section B: beam interactions with materials and atoms*, 247(2):295–306, 2006.
- [132] Garrett J Sykora and Mark S Akselrod. Novel fluorescent nuclear track detector technology for mixed neutron-gamma fields. *Radiation Measurements*, 45(3-6):594–598, 2010.
- [133] JA Bartz, GJ Sykora, E Bräuer-Krisch, and MS Akselrod. Imaging and dosimetry of synchrotron microbeam with aluminum oxide fluorescent detectors. *Radiation Measurements*, 46(12):1936–1939, 2011.
- [134] Go Okada, Brian Morrell, Cyril Koughia, Andy Edgar, Chris Varoy, George Belev, Tomasz Wysokinski, Dean Chapman, and Safa Kasap. Spatially resolved measurement of high doses in microbeam radiation therapy using samarium doped fluorophosphate glasses. *Applied Physics Letters*, 99(12):121105, 2011.
- [135] Matthew D Belley, Ian N Stanton, Mike Hadsell, Rachel Ger, Brian W Langloss, Jianping Lu, Otto Zhou, Sha X Chang, Michael J Therien, and Terry T Yoshizumi. Fiber-optic detector for real time dosimetry of a micro-planar x-ray beam. *Medical physics*, 42(4):1966–1972, 2015.
- [136] James Archer, Enbang Li, Marco Petasecca, Andrew Dipuglia, Matthew Cameron, Andrew Stevenson, Chris Hall, Daniel Hausermann, Anatoly Rosenfeld, and Michael Lerch. X-ray microbeam measurements with a high resolution scintillator fibre-optic dosimeter. *Scientific reports*, 7(1):12450, 2017.
- [137] James Archer, Enbang Li, Marco Petasecca, Andrew Stevenson, Jayde Livingstone, Andrew Dipuglia, Jeremy Davis, Anatoly Rosenfeld, and Michael Lerch. Synchrotron x-ray microbeam dosimetry with a 20 micrometre resolution scintillator fibre-optic dosimeter. *Journal of synchrotron radiation*, 25(3):826–832, 2018.
- [138] Matthew Cameron Marco Petasecca Andrew Stevenson Christopher Hall Daniel Hausermann Anatoly Rosenfeld James Archer, Andrew Dipuglia and Michael Lerch. High spatial resolution scintillator dosimetry of synchrotron microbeams. *Scientific reports*, page in press, 2019.

- 1
2
3
4
5
6
7
8 [139] J Livingstone, J-F Adam, A Stevenson, CJ Hall, D Pelliccia, and
9 D Häusermann. Characterisation of a synthetic diamond detector for
10 1845 experimental dosimetry in mrt. In *Medical Applications of Synchrotron
11 Radiation MASR 2015*, 2015.
- 12 [140] Marco Marinelli, G Prestopino, C Verona, and G Verona-Rinati. Exper-
13 imental determination of the ptw 60019 microdiamond dosimeter active
14 area and volume. *Medical physics*, 43(9):5205–5212, 2016.
- 15 [141] Duncan J Butler, Toby Beveridge, Joerg Lehmann, Christopher P Oliver,
16 1850 Andrew W Stevenson, and Jayde Livingstone. Spatial response of syn-
17 thetic microdiamond and diode detectors measured with kilovoltage syn-
18 chrotron radiation. *Medical physics*, 45(2):943–952, 2018.
- 19 [142] S Almagia, Marco Marinelli, E Milani, G Prestopino, A Tucciarone,
20 21 1855 C Verona, G Verona-Rinati, M Angelone, M Pillon, I Dolbnya, et al.
22 Chemical vapor deposition diamond based multilayered radiation detec-
23 tor: Physical analysis of detection properties. *Journal of applied physics*,
24 107(1):014511, 2010.
- 25 [143] Anders Brahme. Dosimetric precision requirements in radiation therapy.
26 27 1860 *Acta Radiologica: Oncology*, 23(5):379–391, 1984.
- 28 [144] BJ Mijnheer, JJ Battermann, and A Wambersie. What degree of ac-
29 curacy is required and can be achieved in photon and neutron therapy?
30 *Radiotherapy and Oncology*, 8(3):237–252, 1987.
- 31 [145] ICRU Report 24. *Determination of absorbed dose in a patient irradiated*
32 33 1865 *by beams of X or gamma rays in radiotherapy procedures*. International
34 Commission on Radiation Units and Measurements, Woodmont Avenue
35 7910, Washington, D.C. 20014, U.S.A., 1976.
- 36 [146] Richard P Hugtenburg, AS Adegunloye, and David A Bradley. X-ray
37 microbeam radiation therapy calculations, including polarisation effects,
38 with the monte carlo code egs5. *Nuclear Instruments and Methods in*
39 1870 *Physics Research Section A: Accelerators, Spectrometers, Detectors and*
40 *Associated Equipment*, 619(1-3):221–224, 2010.
- 41 [147] J Stepanek, H Blattmann, JA Laissue, N Lyubimova, M Di Michiel, and
42 43 1875 DN Slatkin. Physics study of microbeam radiation therapy with psi-
44 version of monte carlo code geant as a new computational tool. *Medical*
45 *physics*, 27(7):1664–1675, 2000.
- 46 [148] W Ralph Nelson, David WO Rogers, and H Hirayama. The egs4 code
47 system. Technical report, 1985.
- 48 [149] I. Orion, A. B. Rosenfeld, F. A. Dilmanian, F. Telang, B. Ren, and Y. Na-
49 50 1880 mito. Monte carlo simulation of dose distributions from a synchrotron-
51 produced microplanar beam array using the EGS4 code system. *Phys.*
52 *Med. Biol.*, 45:2497–2508, 2000.
- 53 [150] M. De Felici, R. Felici, C. Ferrero, A. Bravin, A. Tartari, and M. Gam-
54 baccini. Monte carlo assessment of peak-to-valley dose ratio for MRT.

- 1
2
3
4
5
6
7
8
9
10
11
12
13
14
15
16
17
18
19
20
21
22
23
24
25
26
27
28
29
30
31
32
33
34
35
36
37
38
39
40
41
42
43
44
45
46
47
48
49
50
51
52
53
54
55
56
57
58
59
60
- 1885 *Nuclear Instruments and Methods in Physics Research Section A: Accelerators, Spectrometers, Detectors and Associated Equipment*, 580(1): 489–492, 2007.
- [151] Y Prezado, I Martínez-Rovira, and M Sánchez. Scatter factors assessment in microbeam radiation therapy. *Medical physics*, 39(3):1234–1238, 2012.
- 1890 [152] Stefan Bartzsch, Michael Lerch, Marco Petasecca, Elke Bräuer-Krisch, and Uwe Oelfke. Influence of polarization and a source model for dose calculation in mrt. *Medical physics*, 41(4), 2014.
- [153] M. De Felici, E. A. Siegbahn, J. Spiga, A. L. Hanson, R. Felici, C. Ferrero, A. Tartari, M. Gambaccini, J. Keyriläinen, and E. Bräuer-Krisch. Monte carlo code comparison of dose delivery prediction for microbeam radiation therapy. In *Journal of Physics: Conference Series*, volume 102, page 012005, 2008.
- 1895 [154] Jenny Spiga, EA Siegbahn, E Bräuer-Krisch, Paolo Randaccio, and A Bravin. The geant4 toolkit for microdosimetry calculations: Application to microbeam radiation therapy (mrt). *Medical Physics*, 34(11): 4322–4330, 2007.
- 1900 [155] P Lazarakis, S Incerti, V Ivanchenko, I Kyriakou, D Emfietzoglou, S Corde, A B Rosenfeld, M Lerch, M Tehei, and S Guatelli. Investigation of track structure and condensed history physics models for applications in radiation dosimetry on a micro and nano scale in geant4. *Biomedical Physics & Engineering Express*, 4(2):024001, 2018. URL <http://stacks.iop.org/2057-1976/4/i=2/a=024001>.
- 1905 [156] E. A. Siegbahn, J. Stepanek, E. Bräuer-Krisch, and A. Bravin. Determination of dosimetrical quantities used in microbeam radiation therapy (MRT) with monte carlo simulations. *Medical Physics*, 33(9):3248–3259, September 2006. ISSN 0094-2405. doi: 10.1118/1.2229422.
- [157] Charlotte Debus, Uwe Oelfke, and Stefan Bartzsch. A point kernel algorithm for microbeam radiation therapy. *Physics in Medicine & Biology*, 62(21):8341, 2017.
- [158] H Nettelbeck, G J Takacs, M L F Lerch, and A B Rosenfeld. Microbeam radiation therapy: A monte carlo study of the influence of the source, multislit collimator, and beam divergence on microbeams. *Med. Phys.*, 36(2), 2009.
- 1915 [159] Sergei Kuznetsov. X-ray optics calculator, June 2014. URL <http://www.ipmt-hpm.ac.ru/xcalc/xcalc/intro.php>.
- 1920 [160] Lázló Koblinger Iván Lux. *Monte Carlo PARTICLE Transport Methods: Neutron and Photon Calculations*. CRC Press, 2000.
- [161] DC Irving. The adjoint boltzmann equation and its simulation by monte carlo. *Nuclear Engineering and Design*, 15:273–293, 1971.
- 1925 [162] Thomas Bortfeld, Wolfgang Schlegel, and Bernhard Rhein. Decomposition of pencil beam kernels for fast dose calculations in three-dimensional treatment planning. *Medical physics*, 20(2):311–318, 1993.

- 1
2
3
4
5
6
7
8 [163] TR Mackie, JW Scrimger, and JJ Battista. A convolution method of
9 calculating dose for 15-mv x rays. *Medical physics*, 12(2):188–196, 1985.
- 10 1930 [164] JE O’connor. The variation of scattered x-rays with density in an irradi-
11 ated body. *Physics in Medicine & Biology*, 1(4):352, 1957.
- 12 [165] Åsa K Carlsson and Anders Ahnesjö. Point kernels and superposi-
13 tion methods for scatter dose calculations in brachytherapy. *Physics in*
14 *Medicine & Biology*, 45(2):357, 2000.
- 15 [166] Parham Alaei, Bruce J Gerbi, and Richard A Geise. Evaluation of a model-
16 based treatment planning system for dose computations in the kilovoltage
17 energy range. *Medical physics*, 27(12):2821–2826, 2000.
- 18 [167] Parham Alaei, George Ding, and Huaiqun Guan. Inclusion of the dose
19 from kilovoltage cone beam ct in the radiation therapy treatment plans.
20 *Medical physics*, 37(1):244–248, 2010.
- 21 1940 [168] Stefan Bartzsch and Uwe Oelfke. A new concept of pencil beam dose
22 calculation for 40–200 keV photons using analytical dose kernels. *Medical*
23 *physics*, 40(11), 2013.
- 24 [169] Andreu Badal and Aldo Badano. Accelerating monte carlo simulations
25 of photon transport in a voxelized geometry using a massively parallel
26 graphics processing unit. *Med. Phys.*, 36:4878–4880, 2009.
- 27 1945 [170] Xun Jia, Xuejun Gu, Josep Sempau, Dongju Choi, Amitava Majumdar,
28 and Steve B Jiang. Development of a gpu-based monte carlo dose calcu-
29 lation code for coupled electron–photon transport. *Physics in Medicine*
30 *and Biology*, 55:3077–3086, 2010.
- 31 [171] Xun Jia, Hao Yan, Xuejun Gu, and Steve B. Jiang. Fast monte carlo sim-
32 ulation for patient-specific CT/CBCT imaging dose calculation. *Physics*
33 *in Medicine and Biology*, 57:577–590, 2012.
- 34 [172] Daniel A Low, William B Harms, Sasa Mutic, and James A Purdy. A
35 technique for the quantitative evaluation of dose distributions. *Medical*
36 *physics*, 25(5):656–661, 1998.
- 37 1955 [173] Jean A. Laissue, Hans Blattmann, Marco Di Michiel, Daniel N. Slatkin,
38 Nadia Lyubimova, Raphael Guzman, Werner Zimmermann, Stephan Bir-
39 rer, Tim Bley, Patrick Kircher, Regina Stettler, Rosmarie Fatzer, Andre
40 Jaggy, Henry Smilowitz, Elke Brauer, Alberto Bravin, Geraldine Le Duc,
41 Christian Nemoz, Michel Renier, William C. Thomlinson, Jiri Stepanek,
42 and Hans-Peter Wagner. Weanling piglet cerebellum: a surrogate for toler-
43 ance to MRT (microbeam radiation therapy) in pediatric neuro-oncology.
44 *Proc. SPIE*, 4508:65–73, 2001. doi: 10.1117/12.450774.
- 45 1960 [174] Raphaël Serduc, Pascale Vérant, Jean-Claude Vial, Régine Farion, Linda
46 Rocas, Chantal Rémy, Taoufik Fadlallah, Elke Brauer, Alberto Bravin,
47 Jean Laissue, Hans Blattmann, and Boudewijn van der Sanden. In vivo
48 two-photon microscopy study of short-term effects of microbeam irradi-
49 ation on normal mouse brain microvasculature. *International Journal of*
50 *Radiation Oncology*Biophysics*Physics*, 64(5):1519–1527, April 2006. ISSN
51 0360-3016. doi: 10.1016/j.ijrobp.2005.11.047.
- 52 1970

- 1
2
3
4
5
6
7
8 [175] Andrzej Niemierko. Reporting and analyzing dose distributions:
9 A concept of equivalent uniform dose. *Medical Physics*, 24(1):
10 103–110, 1997. ISSN 2473-4209. doi: 10.1118/1.598063. URL
11 <http://dx.doi.org/10.1118/1.598063>.
12
- 13 [176] Juergen Meyer, Robert D Stewart, Daniel Smith, James Eagle, Eunsin
14 Lee, Ning Cao, Eric Ford, Reza Hashemian, Jan Schuemann, Jatinder
15 Saini, et al. Biological and dosimetric characterisation of spatially frac-
16 tionated proton minibeam. *Physics in Medicine & Biology*, 62(24):9260,
17 2017.
- 18 [177] I Martínez-Rovira, J Sempau, and Y Prezado. Monte carlo-based treat-
19 ment planning system calculation engine for microbeam radiation therapy.
20 *Medical physics*, 39(5):2829–2838, 2012.
- 21
22 [178] Rolf Bendl, J Pross, A Hoess, M Keller, K Preiser, and W Schlegel.
23 Virtuos-a program for virtual radiotherapy simulation and verification.
24 In *Proc of 11th Int. Conf. on The Use of Computers in Radiation Ther-*
25 *apy, AR Hounsell ua Manchester: North Western Med. Physics Dept*,
26 pages 226–227, 1994.
- 27
28 [179] Christopher M Poole, Liam RJ Day, Peter AW Rogers, and Jeffrey C
29 Crosbie. Synchrotron microbeam radiotherapy in a commercially available
30 treatment planning system. *Biomedical Physics & Engineering Express*, 3
31 (2):025001, 2017.
- 32
33 [180] F Avraham Dilmanian, Gerard M Morris, and James F Hainfeld. Methods
34 for implementing microbeam radiation therapy, March 20 2007. US Patent
35 7,194,063.
- 36
37 [181] Y Prezado, G Fois, G Le Duc, and A Bravin. Gadolinium dose enhance-
38 ment studies in microbeam radiation therapy. *Medical physics*, 36(8):
39 3568–3574, 2009.
- 40
41 [182] I Martínez-Rovira and Y Prezado. Monte carlo dose enhancement studies
42 in microbeam radiation therapy. *Medical physics*, 38(7):4430–4439, 2011.
- 43
44 [183] Gurdal Gokeri, Cemil Kocar, and Mehmet Tombakoglu. Monte carlo sim-
45 ulation of microbeam radiation therapy with an interlaced irradiation ge-
46 ometry and an au contrast agent in a realistic head phantom. *Physics in*
47 *Medicine & Biology*, 55(24):7469, 2010.
- 48
49 [184] Wan Nordiana Rahman, Christopher James Wong, Naoto Yagi, Robert
50 Davidson, and Moshi Geso. Dosimetry and its enhancement using gold
51 nanoparticles in synchrotron based microbeam and stereotactic radio-
52 surgery. In *AIP Conference Proceedings*, volume 1266, pages 107–110.
53 AIP, 2010.
- 54
55 [185] Wan Nordiana Rahman, Robert Davidson, Naoto Yagi, Vipul Bansal,
56 Moshi Geso, and Ian Darby. Influence of gold nanoparticles on radiation
57 dose enhancement and cellular migration in microbeam-irradiated cells.
58 *BioNanoScience*, 1(1-2):4–13, 2011.

- 1
2
3
4
5
6
7
8 [186] Imen Miladi, Christophe Alric, Sandrine Dufort, Pierre Mowat, Aurélie
9 2015 Dutour, Céline Mandon, Gautier Laurent, Elke Bräuer-Krisch, Nirmitha
10 Herath, Jean-Luc Coll, et al. The in vivo radiosensitizing effect of gold
11 nanoparticles based mri contrast agents. *Small*, 10(6):1116–1124, 2014.
- 12
13 [187] Géraldine Le Duc, Imen Miladi, Christophe Alric, Pierre Mowat, Elke
14 2020 Bräuer-Krisch, Audrey Bouchet, Enam Khalil, Claire Billotey, Marc
15 Janier, François Lux, et al. Toward an image-guided microbeam radi-
16 ation therapy using gadolinium-based nanoparticles. *ACS nano*, 5(12):
17 9566–9574, 2011.
- 18
19 [188] Géraldine Le Duc, Stéphane Roux, Amandine Paruta-Tuarez, Sandrine
20 2025 Dufort, Elke Brauer, Arthur Marais, Charles Truillet, Lucie Sancey, Pascal
21 Perriat, François Lux, et al. Advantages of gadolinium based ultrasmall
22 nanoparticles vs molecular gadolinium chelates for radiotherapy guided
23 by mri for glioma treatment. *Cancer nanotechnology*, 5(1):4, 2014.
- 24
25 [189] Sandrine Dufort, Géraldine Le Duc, Murielle Salomé, Valerie Bentivegna,
26 2030 Lucie Sancey, Elke Bräuer-Krisch, Herwig Requardt, François Lux, Jean-
27 Luc Coll, Pascal Perriat, et al. The high radiosensitizing efficiency of a
28 trace of gadolinium-based nanoparticles in tumors. *Scientific reports*, 6:
29 29678, 2016.
- 30
31 [190] Elette Engels, Stéphanie Corde, Sally McKinnon, Sébastien Incerti, Kon-
32 2035 stantin Konstantinov, Anatoly Rosenfeld, Moeava Tehei, Michael Lerch,
33 and Susanna Guatelli. Optimizing dose enhancement with ta 2 o 5
34 nanoparticles for synchrotron microbeam activated radiation therapy.
Physica Medica, 32(12):1852–1861, 2016.
- 35
36 [191] Robert J Griffin, Nathan A Koonce, Ruud P M Dings, Eric Siegel, Ed-
37 2040 uardo G Moros, Elke Bräuer-Krisch, and Peter M Corry. Microbeam
38 radiation therapy alters vascular architecture and tumor oxygenation and
39 is enhanced by a galectin-1 targeted anti-angiogenic peptide. *Radiation
40 research*, 177(6):804–812, 2012.
- 41
42 [192] M Donzelli, E Bräuer-Krisch, and U Oelfke. Brain motion induced arte-
43 2045 facts in microbeam radiation therapy: a monte carlo study. *Radiotherapy
44 and Oncology*, 118:S34–S35, 2016.
- 45
46 [193] Elena Eggl, Martin Dierolf, Klaus Achterhold, Christoph Jud, Benedikt
47 Günther, Eva Braig, Bernhard Gleich, and Franz Pfeiffer. The munich
48 compact light source: initial performance measures. *Journal of syn-
49 chrotron radiation*, 23(5):1137–1142, 2016.
- 50
51 [194] Michael D Wright. Microbeam radiosurgery: an industrial perspective.
52 2050 *Physica Medica*, 31(6):601–606, 2015.
- 53
54 [195] Roderick Loewen. A compact light source: design and technical feasibil-
55 ity study of a laser-electron storage ring x-ray source. Technical report,
56 Stanford Linear Accelerator Center, Menlo Park, CA (US), 2004.
- 57
58 [196] Karin Burger, Katarina Ilicic, Martin Dierolf, Benedikt Günther, Diet-
59 2055 rich WM Walsh, Ernst Schmid, Elena Eggl, Klaus Achterhold, Bernhard
60

- 1
2
3
4
5
6
7
8 Gleich, Stephanie E Combs, et al. Increased cell survival and cytogenetic
9 integrity by spatial dose redistribution at a compact synchrotron x-ray
10 source. *PloS one*, 12(10):e0186005, 2017.
- 11
12 2060 [197] K. Burger, K. Ilicic, A. Hunger, M. Dierolf, B. Günther, E. Schmid,
13 D. W. M. Walsh, T. Urban, S. Bartzsch, A. Radtke, E. Eggl, K. Achter-
14 hold, B. Gleich, S. E. Combs, M. Molls, T. E. Schmid, F. Pfeif-
15 fer, and J. J. Wilkens. Microbeam radiation therapy at a laser-based
16 compact synchrotron x-ray source. In *2017 Conference on Lasers*
17 *and Electro-Optics Europe European Quantum Electronics Conference*
18 *(CLEO/Europe-EQEC)*, pages 1–1, June 2017.
- 19
20 [198] Annique C. Dombrowsky, Karin Burger, Ann-Kristin Porth, Marlon Stein,
21 Martin Dierolf, Benedikt Günther, Klaus Achterhold, Bernhard Gleich,
22 Annette Feuchtinger, Stefan Bartzsch, Elke Beyreuther, Stephanie E.
23 2070 Combs, Franz Pfeiffer, Jan Wilkens, and Thomas E. Schmid. proof of princi-
24 ple experiment for microbeam radiation therapy at the munich compact
25 light source. *submitted*, 2019.
- 26 [199] Marie Jacquet and Pekka Suortti. Radiation therapy at compact compton
27 sources. *Physica Medica*, 31(6):596–600, 2015.
- 28
29 2075 [200] Kerry Babcock, Narinder Sidhu, Vijayananda Kundapur, and Kaiser Ali.
30 Collimator design for experimental minibeam radiation therapy. *Medical*
31 *physics*, 38(4):2192–2197, 2011.
- 32
33 [201] Soha Bazyar, Christina R Inscoc, E Timothy O’Brian, Otto Zhou, and
34 Yueh Z Lee. Minibeam radiotherapy with small animal irradiators; in
35 2080 vitro and in vivo feasibility studies. *Physics in Medicine & Biology*, 62
36 (23):8924, 2017.
- 37
38 [202] John Wong, Elwood Armour, Peter Kazanzides, Iulian Iordachita, Erik
39 Tryggstad, Hua Deng, Mohammad Matinfar, Christopher Kennedy, Ze-
40 jian Liu, Timothy Chan, et al. High-resolution, small animal radiation
41 2085 research platform with x-ray tomographic guidance capabilities. *Interna-*
42 *tional Journal of Radiation Oncology* Biology* Physics*, 71(5):1591–1599,
43 2008.
- 44
45 [203] Y Prezado, M Dos Santos, W Gonzalez, G Jouvion, C Guardiola, S Hein-
46 rich, D Labiod, M Juchaux, L Jourdain, C Sebrie, et al. Transfer of
47 2090 minibeam radiation therapy into a cost-effective equipment for radiobi-
48 ological studies: a proof of concept. *Scientific reports*, 7(1):17295, 2017.
- 49
50 [204] Nolan M Esplen, Lila Chergui, Chris D Johnstone, and Magdalena
51 Bazalova-Carter. Monte carlo optimization of a microbeam collimator
52 design for use on the small animal radiation research platform (sarrp).
53 2095 *Physics in Medicine & Biology*, 63(17):175004, 2018.
- 54
55 [205] Eric C Schreiber and Sha X Chang. Monte carlo simulation of a compact
56 microbeam radiotherapy system based on carbon nanotube field emission
57 technology. *Medical physics*, 39(8):4669–4678, 2012.
- 58
59
60

- 1
2
3
4
5
6
7
8 [206] D Shiffler, O Zhou, C Bower, M LaCour, and K Golby. A high-current,
9 2100 large-area, carbon nanotube cathode. *IEEE transactions on plasma sci-*
10 *ence*, 32(5):2152–2154, 2004.
- 11 [207] F Avraham Dilmanian and Allen G Meek. Heavy ion therapy with mi-
12 crobeams, July 29 2010. US Patent App. 12/692,216.
- 13 [208] M Kłodowska, Paweł Olko, and MPR Waligórski. Proton microbeam ra-
14 2105 diotherapy with scanned pencil-beams–monte carlo simulations. *Physica*
15 *Medica*, 31(6):621–626, 2015.
- 16 [209] Olga Zlobinskaya, Stefanie Girst, Christoph Greubel, Volker Hable, Chris-
17 tian Siebenwirth, Dietrich WM Walsh, Gabriele Multhoff, Jan J Wilkens,
18 Thomas E Schmid, and Günther Dollinger. Reduced side effects by proton
19 microchannel radiotherapy: study in a human skin model. *Radiation and*
20 2110 *environmental biophysics*, 52(1):123–133, 2013.
- 21 [210] Y Prezado and GIOVANNA ROSA Fois. Proton-minibeam radiation ther-
22 apy: A proof of concept. *Medical physics*, 40(3), 2013.
- 23
24
25
26
27
28
29
30
31
32
33
34
35
36
37
38
39
40
41
42
43
44
45
46
47
48
49
50
51
52
53
54
55
56
57
58
59
60